~~Seasonal Variability in In-situ~~ Supraglacial Streamflow and Meteorological Drivers from~~in~~ Southwest Greenland~~in 2016~~

Rohi Muthyala[1], Asa K. Rennermalm[1], Sasha Z. Leidman[1], Matthew G. Cooper[2], Sarah W. Cooley[3~~,4~~], Laurence C. Smith[~~3,~~4,5], Dirk van As[6~~5~~]

[1]Department of Geography, Rutgers, The State University of New Jersey, New Brunswick, NJ, 08901, USA
[2]Atmospheric Sciences and Global Change Division, Pacific Northwest National Laboratory, Richland, WA, 99354, USA
3Department of Earth System Science, Stanford University, Stanford, CA, USA
4[~~3~~]Institute at Brown for Environment and Society, Brown University, Providence, RI, 02912, USA
5[~~4~~]Department of Earth, Environmental, and Planetary Sciences, Brown University, Providence, RI, 02912, USA
6[~~5~~]Geological Survey of Denmark and Greenland, Øster Voldgade 10, 1350 Copenhagen, Denmark

Correspondence to: Rohi Muthyala (rohi.muthyala.91@gmail.com)

Abstract. Greenland ice sheet surface runoff is drained~~evacuated~~ through supraglacial stream networks~~,~~. This evacuation ~~which~~ influences surface mass balance as well as ice dynamics. However, in-situ observations of meltwater discharge through these stream networks are rare. In this study, we present 46 discharge measurements and continuous water level measurements for 62 days spanning 13 June to 13 August, 2016 for a 0.6 km^2 supraglacial stream catchment in southwest Greenland. The result is an unprecedented long record of supraglacial discharge that captures~~ing~~ both diurnal and seasonal variability. ~~By comparing in situ hydraulic geometry parameters with previous studies, we find that significant heterogeneity exists such that estimating stream discharge using these parameters over ungauged supraglacial catchments could lead to substantial errors.~~ A comparison of surface energy fluxes to stream discharge reveals shortwave radiation as the primary driver of melting ~~(78% of melt energy)~~. However, during high melt episodes, the contribution of shortwave radiation~~only contributes to 50%~~ is reduced by ~40% (~~proportion of melt energy reduced~~ from 1.13 to 0.73 proportion). Instead, the relative contribution of longwave radiation, sensible heat, and latent heat fluxes to overall melt increases by ~~16.5%, 4%, and 7%~~ ~24%, 6%, and 10% (proportion increased from -0.32 to -0.08, 0.28 to 0.34, and -0.04 to 0.06) respectively. Our data also identify~~show~~ a seasonal variation in the timing of daily maximum discharge during clear sky days, shifting from 16:00 local time (i.e., 2~~.75~~ hours 45 minutes after solar noon) in late June to 14:00 in late July, then rapidly returning~~s~~ to 16:00 in early August. ~~coincident with an abrupt drop in air temperature. These changes in peak daily flow timing can be attributed to a changing effective catchment area, resulting in a smaller stream network supplying water to the outlet at the end of the season throughout the melt season.~~ The change in timing of daily maximum discharge could be attributed to the expansion and contraction of the stream network, caused by probable freezing skin temperatures at night. The abrupt shift, in early August, in the timing of daily maximum discharge coincides with a drop in air temperature, water temporarily stored in weathering crust, and reduced importance of stream

velocity in controlling discharge. Further work is needed to investigate if these results can be transferable to larger catchments and uncover how widespread rapid shifts in the timing of peak discharge are~~is~~ across Greenland supraglacial streams, and thus their potential impact on meltwater delivery to the subglacial system and ice dynamics.

1 Introduction

Mass loss from the Greenland ice sheet increased six-fold from the 1980s to the 2010s (286±20 Gt yr^{-1}) (Mouginot et al., 2019~~; Shepherd et al., 2019; Velicogna et al., 2020~~). This mass loss was dominated by enhanced surface melting and runoff (v~~V~~an den Broeke et al., 2016). The increase in runoff raised Greenland's contribution to global sea-level rise from less than 5% in 1993 to more than 25% in 2014 (Chen et al., 2017). Increased surface melting also influences ice sheet basal properties (Das et al., 2008; Colgan et al., 2011;~~ Bell et al., 2017; Kingslake et al., 2017;~~ Flowers, 2018), and ice dynamics (~~V~~van de Wal et al., 2008; Shepherd et al., 2009; Schoof, 2010; Hoffmann et al., 2011; Hewitt, 2013; Andrews et al., 2014~~5~~). Though the net effect of meltwater runoff on basal pressures, and ice velocities remains unclear, recent studies show that, in the lower ablation regions, increase in surface runoff results in a decrease in ice velocities (Sundal et al., 2011; Tedstone et al., 2015; Davison et al., 2019). For example, a 50% increase in surface melting during 2007-2014, compared to 1985-1994, resulted in 12% slower ice flow in the lower ablation region (within ~50 km of the margin) of west Greenland (Tedstone et al., 2015). Surface melting feeds numerous supraglacial stream/river drainage networks that develop on the surface of the Greenland ice sheet ablation zone (Smith et al., 2015; 2017; Yang and Smith, 2013; 2016; Pitcher and Smith, 2019). These networks transport runoff sourced from melting ice, snow, and/or slush within the stream catchment (Holmes, 1955; Karlstrom et al., 2014), and often terminate in moulins, from wherein meltwater moves within and beneath the ice sheet before emerging in proglacial rivers, lakes, fjords, and the ocean (Chu, 2014; Rennermalm et al., 2013). Despite the importance of Greenland's surface runoff to ~~surface mass balance~~ ice sheet dynamics and sea level rise, only a handful of studies use~~ing~~ in situ supraglacial stream discharge to characterize current conditions (Holmes, 1955; Chandler et al., 2013; McGrath et al., 2011; ~~Smith et al., 2015;~~ Gleason et al., 2016; Smith et al., 2015, 2017, 2021; Chandler et al., 2021), and these studies are limited to short periods except for Wadham et al. (2016), which recorded a 50-days period of supraglacial discharge as a part of their study on export of nitrogen from Greenland ice sheet.~~(a couple of days to a maximum of 15 days).~~

~~Every melting season, numerous supraglacial stream/river drainage networks~~ that ~~develop on the surface of the Greenland ice sheet ablation zone (Smith et al., 2015; 2017; Yang and Smith, 2013; 2016; Pitcher and Smith, 2019). These networks transport runoff sourced from melting ice, snow, and/or slush within the stream catchment (Holmes, 1955; Karlstrom et al., 2014), and often terminate in moulins, from where~~in ~~meltwater moves within and beneath the ice sheet before emerging in proglacial rivers, lakes, fjords, and the ocean (Chu, 2014; Rennermalm et al., 2013).~~

Supraglacial stream discharge varies seasonally in concert with surface melting, with low flow in the beginning and end of the melt~~ing~~ season and higher flow in the middle of the melt~~ing~~ season (Holmes, 1955). Supraglacial discharge also shows a pronounced diurnal variation (McGrath et al., 2011; Wadham et al., 2016; Smith et al., 2017, 2021; Yang et al., 2018). While daily maximum discharge varies with catchment size and day of the season, discharge decreases when melt energy drops off at night (Marston ~~et al.~~, 1983; Mernild et al., 2006; McGrath et al., 2011; Yang et al., 2018). Diurnal variability and timing of meltwater delivery to the subglacial drainage system have been shown to influence ice sheet velocities in several studies (Bartholomew et al., 2012; Sole et al., 2013; Andrews et al., 2014; Smith et al., 2021~~0~~), with up to 65% increase in ice velocity in the lower ablation area (Sole et al., 2013). Short-term speed-ups occur in the lower ablation regions of southwest Greenland (Shepherd et al., 2009), with an increase in ice velocities up to 300-400% (compared to pre-melt speeds) that lasts for a few days to a week in response to the variations in surface runoff supply (Sole et al., 2013). However, no observational studies have documented diurnal variability and timing of Greenland ice sheet supraglacial flow throughout an entire melt season.

The routing of meltwater through supraglacial stream networks as well as non-channelized surfaces delays the timing of peak discharge at the moulin relative to the timing of peak surface melt (Karlstrom et al., 2014; Yang et al., 2018). This peak time lag depends on the size of the catchment and meltwater routing time (Holmes, 1955; Mernild et al., 2006; McGrath et al., 2011; Smith et al., 2017). Larger catchments imply a longer stream network, and thus a larger time lag between peak surface melt and peak discharge, compared to smaller catchments with similar surface melt intensity. Additionally, when a supraglacial stream network grows and shrinks throughout the melt season the magnitude of peak moulin discharge decreases and increases respectively (Yang et al., 2018) ~~the seasonal evolution of a supraglacial stream network can alter the magnitude and timing of peak moulin discharge~~. For example, ~~as~~ when the actively flowing network contracts ~~through the season~~ (Lampkin and VanderBerg, 2014), and more water is transported via porous media flow, the peak time lag increases, and the magnitude of peak moulin discharge decreases by more than 50% (Yang et al., 2018). ~~The magnitude and timing of peak moulin discharge may also be influenced by the temporary storage of meltwater~~ Non-channelized meltwater predominantly flows or is temporarily stored in the weathering crust (Cooper et al., 2018; Yang et al., 2018). Weathering crust is a degraded, porous surface layer of ice that retains meltwater temporarily, influencing the magnitude of peak discharge (14-18 cm of specific melt water storage within low density ice; Cooper et al., 2018) and promoting~~es~~ subsurface flow (Karlstrom et al., 2014; Cooper et al., 2018).~~, and therefore~~ This may slow the transport of meltwater to supraglacial streams (Munro, 2011; Karlstrom et al., 2014; Cook et al., 2016; Yang et al., 2018; Gleason et al., 2021), delaying the time of peak discharge. In addition to the structure of weathering crust, the amount of melt water stored is proportional to solar radiation as windy and overcast conditions with higher longwave radiation reduce the storage capacity of weathering crust (Takeuchi, 2000). However, the seasonal evolution of timing of peak discharge and storage of meltwater in weathering crust through the melt season has never been reported in previous studies due to the short span of in situ data available.

In Greenland's ablation zone, ~~the~~ seasonal and interannual variability in meltwater production~~, thereby surface runoff,~~ is primarily driven by the variability in~~of the absorption of~~ shortwave radiation absorption (v~~V~~an den Broeke et al., 2011; Ryan et al., 2019). Secondary melt drivers are turbulent fluxes of sensible and latent heat, particularly in the lower ablation zone of southwest Greenland (~~V~~van den Broeke et al., 2011;~~,~~ Fausto et al. 2016). Lesser~~Additional~~ drivers include~~are~~ anomalously moist and warm air masses advected over the ice sheet by atmospheric rivers (Mattingly et al., 2018), and clouds with contrasting feedback to surface melt (Bennartz et al., 2013). While a few studies report an increase in cloud cover enhances downward longwave radiation and hence melt (Van Tricht et al., 2016; Gallagher et al., 2020; Izeboud et al., 2020), others show that it also limits ~~the~~ shortwave radiation, thus decreasing summer melt in ablation areas (Hofer et al., 2017; Izeboud et al., 2020). It remains unclear which of these radiation components dominantly drives surface melt through clouds over the Greenland ice sheet. Numerous studies examine the linkages between surface energy balance, surface melting, and runoff using regional climate models (e.g. Fettweis et al., 2017; Noel et al., 2018), and automatic weather station data (van As et al., 2012). In contrast to model simulated surface melt and runoff, observed meltwater delivery to moulins (i.e. supraglacial discharge) is affected by processes influencing surface flow and storage of water in the weathering crust. However, ~~but~~ relatively few compare surface energy fluxes with in situ observations of supraglacial stream discharge in Greenland (Smith et al., 2017) and no study compares their contribution to in situ stream discharge throughout the melt season. In contrast to simulated surface melt, observed runoff is affected by processes influencing surface flow and storage of water from when it melts to when it is delivered to the moulin, and thus a better representation of meltwater that actually leaves the ice sheet surface.

Understanding supraglacial stream channel geometry is critical for determining the routing speed and the spatial extent of meltwater for the absorption of incoming solar radiation (Karlstrom and Yang, 2016; Leidman et al., 2021). Smith et al. (2015) and Gleason et al., (2016)~~, examine how Greenland supraglacial streams can be characterized with hydraulic geometry principles. In terrestrial hydrology,~~ at-a-station hydraulic geometry theory to calculate how~~holds that~~ channel width, depth, and velocity co-vary nonlinearly with discharge for a fixed stream cross-section (Leopold and Maddock, 1953; Ferguson, 1986; Gleason et al., 2015). This theory provides a set of equations with parameters that can be generalized to estimate discharge in ungauged rivers (Smith et al., 1996; 2015; Ashmore and Sauks, 2006; Andreadis et al., 2020). Similarly, a generalization of supraglacial streams' hydraulic geometries would open possibilities for scaling and modeling discharge. For example, Smith et al. (2015) used field-calibrated hydraulic geometry to estimate instantaneous discharges in 523 moulins in southwestern Greenland, yielding values ranging from 0.36 to 17.72 m^{3}s^{-1} with a mean value of 3.15 m^{3}s^{-1}. In contrast, Gleason et al. (2016) and Smith et al. (2017) argued that unlike terrestrial systems, uniform hydraulic behavior cannot necessarily be expected from an ice substrate. ~~However, o~~Only a few studies have quantified hydraulic geometry of supraglacial streams, all using a relatively short data record.

In light of the current knowledge gaps in Greenland ice sheet supraglacial hydrology discussed above, this paper addresses the following questions: (i) how does supraglacial discharge vary over an entire melt season within a well-defined catchment? (ii) what drives these variations throughout the melt season? (iii) do the timing and magnitude of daily peak discharge change throughout the season as modeled by Yang et al. (2018)? (iv) and, if so, do the observed changes correspond to changing hydraulic geometry parameters in the supraglacial stream channel? ~~In this study, w~~We present a 62-day time series of supraglacial streamflow, in southwest Greenland, spanning most of the 2016 melt~~ing~~ season (13 June – 13 August, 2016) ~~in terms of total meltwater production~~. The supraglacial stream drainage network was mapped using unmanned aerial vehicle (UAV) imagery and field~~manual~~ GPS observations.~~, and s~~Surface energy fluxes were calculated or measured using meteorological observations from a nearby automatic weather station (KAN_L). From~~Using~~ these data, we examine supraglacial stream discharge diurnal variability, daily maximum and uncertainties, and the contributions of meteorological drivers to this discharge throughout the melt season. ~~covariance between discharge and surface energy balance drivers, seasonal changes in daily peak discharge timing, and hydraulic geometry parameters. Finally, we compare our hydraulic geometry parameters to previous work on supraglacial streams.~~ We also estimate and compare hydraulic geometry parameters of the supraglacial stream from our catchment with previous studies. Finally we explore how time of daily maximum discharge evolves through the melt season. We conclude with a discussion of how change in time of daily maximum discharge varies with air temperature, hydrologic geometry parameters, and subsurface water level, and some recommendations for future research.

2 Study Area

The study area is a 0.6 km^2 internally drained supraglacial catchment in southwest Greenland, hereafter called “~~‘~~660 catchment~~’~~” (after “Point 660” where a gravel road from the town of Kangerlussuaq ends at the ice sheet margin). The catchment is located ~1–2 km upstream of the ice edge between two outlet glaciers, Isunnguata Sermia and Russell Glacier, and roughly 35 km east of ~~the town of~~ Kangerlussuaq (Fig. 1). The stream network terminates in a moulin (location 67.1562°N, 50.0064°W in 2016). ~~About 850 m upstream of the moulin, a gauging station for monitoring water level and discharge was installed at 67.1573°N, 49.9951°W.~~ Elevations in the catchment span from 610 m near the gauging station to 660 m (above the WGS84 ellipsoid) at the catchment's highest point (Fig. 1).

The catchment surface consists of a rugged bare-ice landscape with small supraglacial ponds and an incised stream network (Fig. 2a). The ~~clean~~ bare-ice surface ~~with minimal impurities~~ has an albedo of 0.57±0.04 (Moustafa et al., 2015) and has~~had~~ a thin (~0.1–0.3 m) surface layer of weathering crust comprising porous ice and cryoconite holes (Fig. 2c). These cryoconite holes are partially filled with water and accumulate “cryoconite,” consisting of dust, sediment, and biological matter (Takeuchi~~ et al.~~, 2000; Cooper et al., 2018~~9~~). Cryoconite deposits are widespread in streams and ponds throughout the catchment (Leidman et al., 2021). The catchment is situated in a region where winter snow accumulation is relatively low, and that experiences extensive melting from June through August so that little to no snow cover remains on the bare ice early in the melt~~ing~~ season (Rennermalm et al., 2013; Ryan et al., 2019).

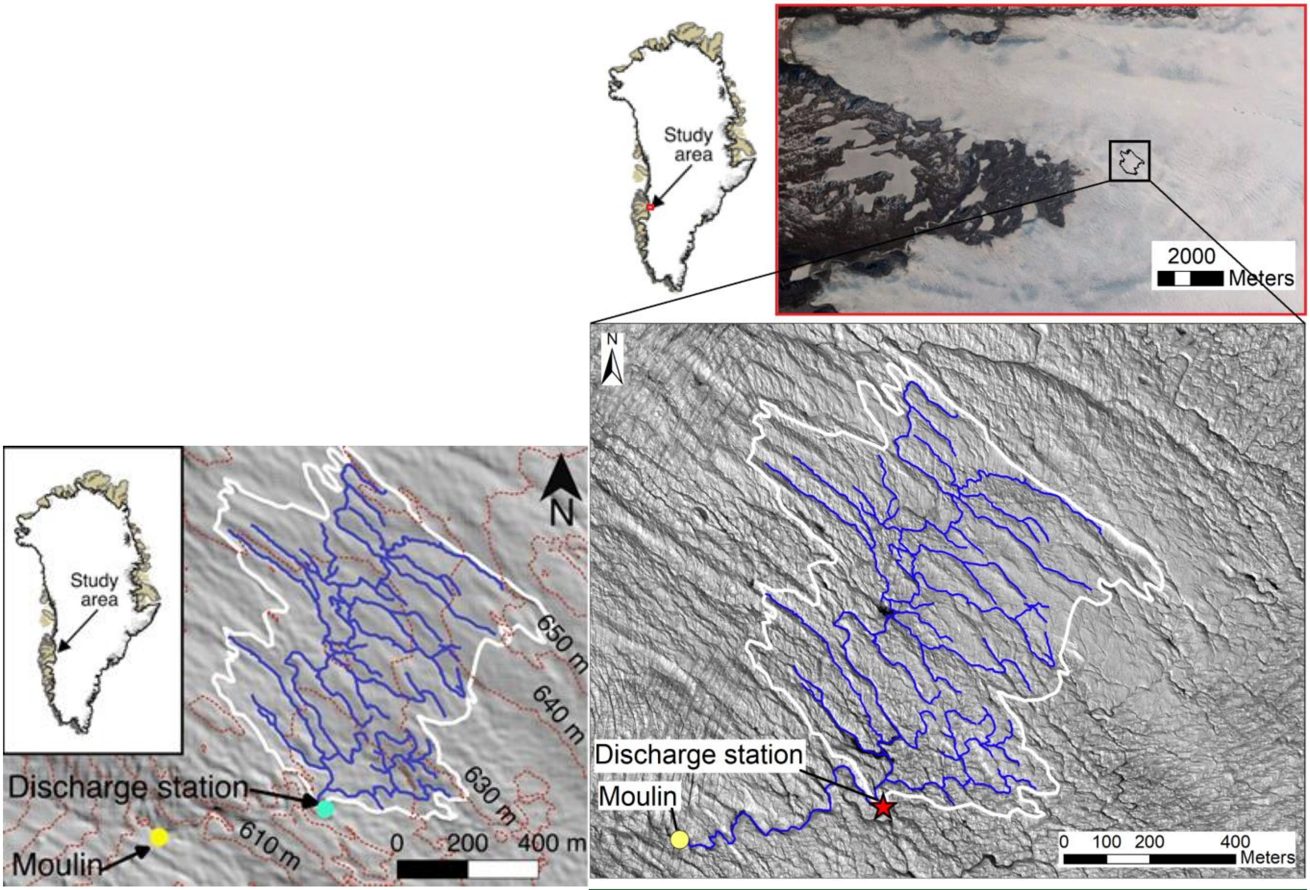

Figure 1: Map of study site showing the supraglacial catchment boundary (white), streams of order 1, 2, and 3 (blue), and locations of the discharge station and terminal~~the~~ moulin. ~~Red contour lines are derived using a 10 m Arctic DEM from Polar Geospatial Center (PGC). Hillshading is generated from a PGC 2m DEM.~~

3 Data and methods

3.1 Supraglacial stream discharge

About 850 m upstream of the moulin, a gauging station for monitoring water level and discharge was installed at 67.1573°N, 49.9951°W. ~~Supraglacial stream discharge was calculated for 62 days from 13 June to 13 August 2016. Discharge was determined with a rating curve relating 46~~ discrete~~occasional discharge measurements to continuous (5 min interval) observations of stream water stage.~~ Stream water stage was measured ~~every 5 min~~ using a setup of two Solinst ~~loggers (~~pressure transducers~~)~~:~~,~~ a Levelogger® ~~-~~in a perforated, weighted steel enclosure resting on the stream bed tied to an embedded pole (Fig. 2b), which also supplies a fixed reference point throughout the season, and a Barologger~~-~~® (Solinst, 2020) installed 25–30 m northeast of the gauging/discharge station. Stage is calculated after barometric pressure correction, yielding a continuous time series of stage measurements, recorded every 5 minutes from 13 June to 13 August 2016.

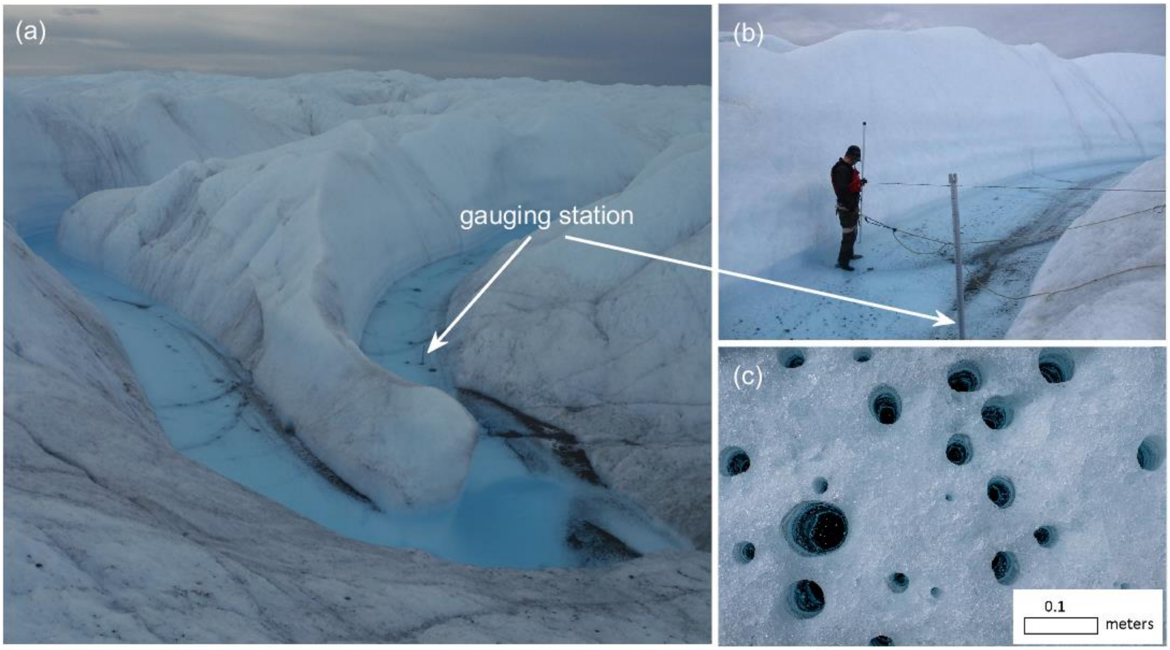

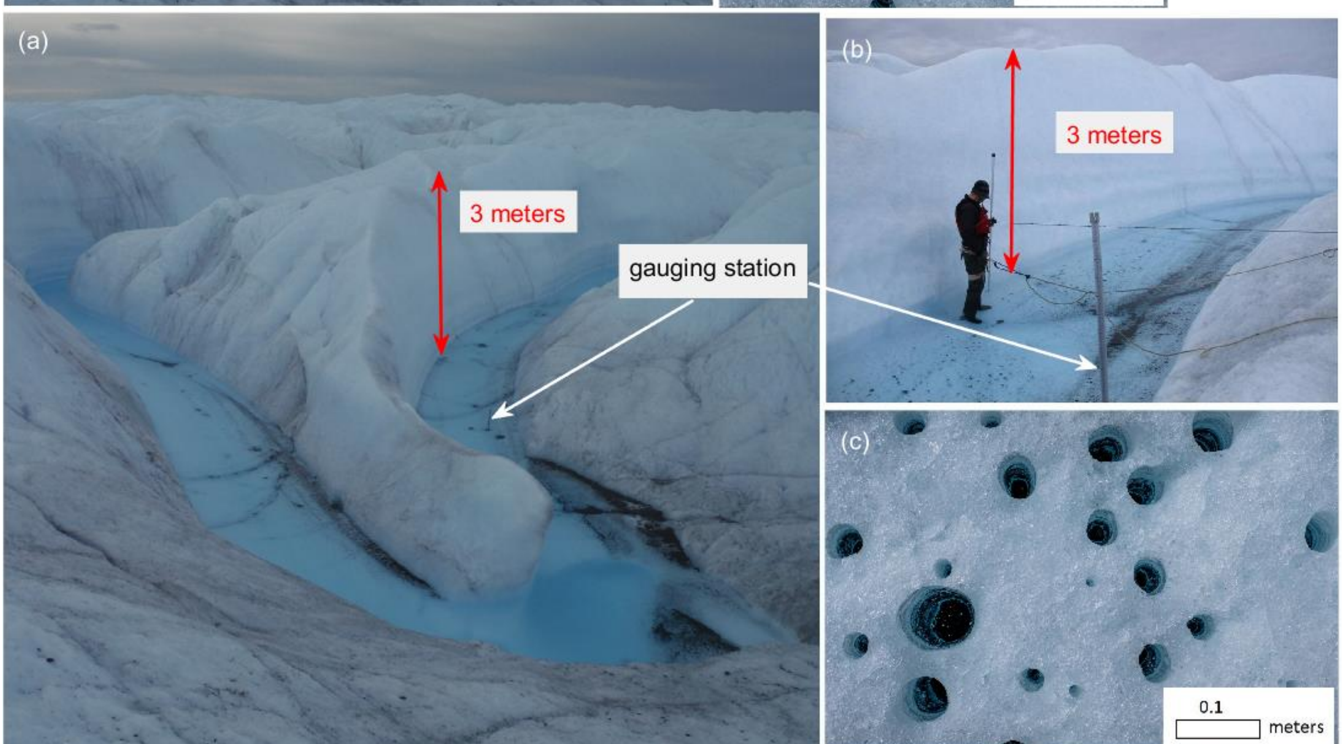

Figure 2: (a) ~~The main stem of the s~~Supraglacial stream main stem~~,~~ and ~~location of the~~ gauging station location. (b) Close up photo of the stream cross-section, and the gauging station during discharge measurement. (c) Cryoconite holes on the bare ice surface vary from 0.02–0.08 m in diameter and 0.1–0.3 m in depth (in this figure). These holes are partially water filled and contain cryoconite (biological matter~~)~~, dust, and sediment) at the bottom.

Discharge was calculated with the velocity-area method using inputs of cross-sectional area and stream water velocity (e.g. Herschy, 1993a). Stream velocity was measured at 60% of the depth at each 0.2 m interval horizontally across the stream, with either a General Oceanics current meter or Price Type-AA current meter. Cross-sections of stream depth were measured at 0.2 m intervals across the 1.7–3.3 m wide stream. In total, 46 discrete observations of velocity and cross-sectional area were made, including 27 measured every hour from 15:30 on 26 July 2016 to 17:30 on 27 July 2016 (local time) to capture the entire diurnal range. The remaining 19 observations were collected over the entire study period and sampled on average every 3–7 days between 12:00 to 17:00 local time. ~~Cross-sections of stream depth were measured at 0.2 m intervals across the 1.7–3.3 m wide stream.~~ Though measurements were collected in the same location throughout the season, continuous thermal erosion of the bed resulted in small changes in cross-sectional geometry (Fig. 3a), consistent with previous studies (Wadham et al., 2016; Smith et al., 2021), that measured long-term supraglacial stream discharge. The hourly measurements were collected with a fixed reference start point over a 26-hour period. ~~Stream velocity was measured at 60% of the depth at each 0.2 m interval at 60% of the depth, horizontally across the stream, with either a General Oceanics current meter or Price Type-AA current meter.~~

The discharge rating curve was generated with a best fit power-law (e.g. Herschy, 1993b):

$$Q = p(H + \alpha)^{\beta} \tag{1}$$

where p and β are constants estimated by fitting the curve to observations of discharge (Q) and water level, also called stage height (H), and α is the water level sensor offset from the stream bottom. In this study, the box with the ~~level logger~~ Levelogger® was placed on the stream bed ~~and therefore~~ (α=0).

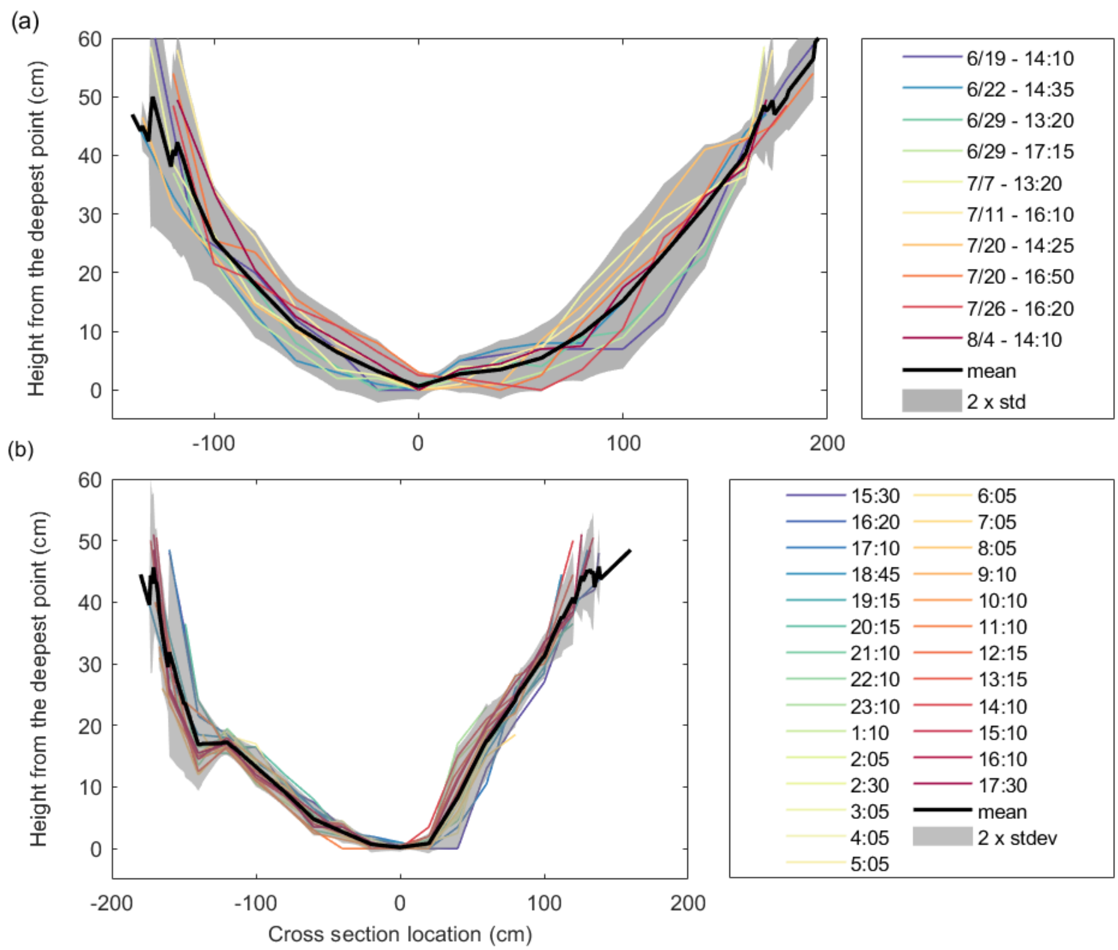
(a)
Height from the deepest point (cm)
6/19 - 14:10
6/22 - 14:35
6/29 - 13:20
6/29 - 17:15
7/7 - 13:20
7/11 - 16:10
7/20 - 14:25
7/20 - 16:50
7/26 - 16:20
8/4 - 14:10
mean
2 x std
(b)
Height from the deepest point (cm)
Cross section location (cm)
15:30
16:20
17:10
18:45
19:15
20:15
21:10
22:10
23:10
1:10
2:05
2:30
3:05
4:05
5:05
6:05
7:05
8:05
9:10
10:10
11:10
12:15
13:15
14:10
15:10
16:10
17:30
mean
2 x stdev

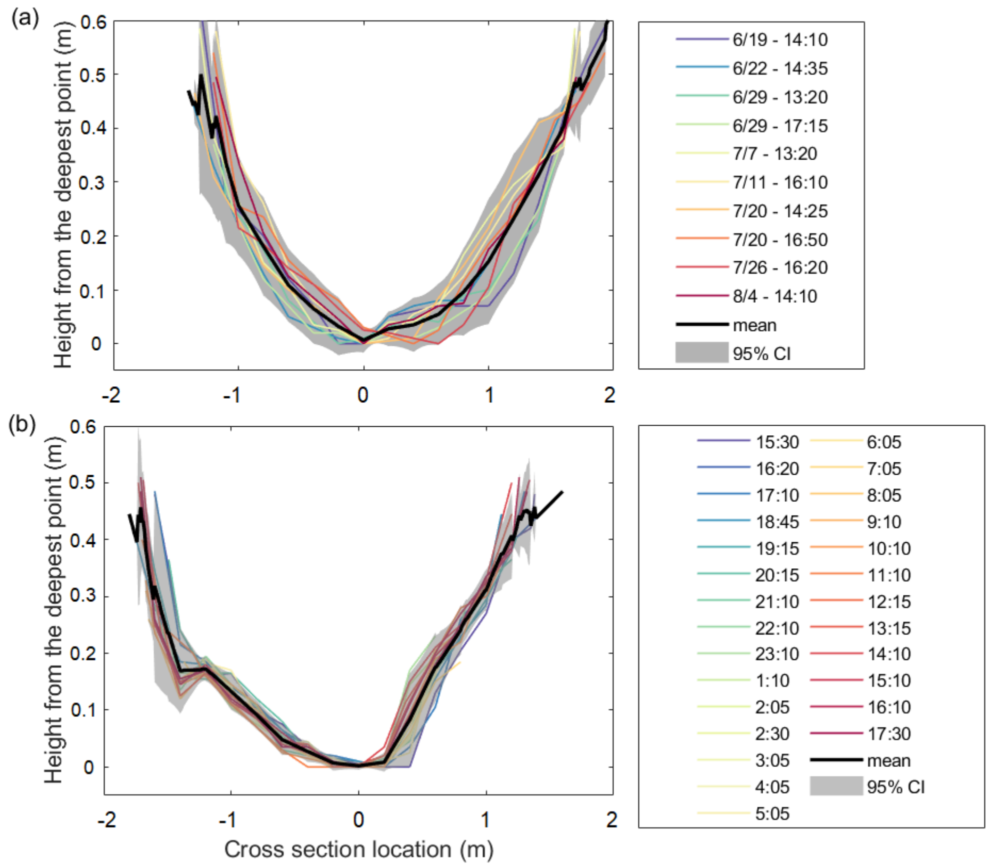

Figure 3: Stream cross-section depth profiles along the wetted perimeter: (a) daily cross-sections using measurements performed during 19 June through 8 August, with samples collected on average every 3–7 days, and (b) hourly cross-sections using measurements from 15:30 on 26 July to 17:30 on 27 July 2016; These depth profiles are made with the maximum depth as a point of reference in each sample. The mean profile is shown in a thick black line and uncertainty (95% CI~~2 x standard deviation~~) is shown in the grey shaded area. All times correspond to local time.

Discharge was determined using a rating curve relating 46 discrete discharge measurements to continuous (5-min interval) observations of stream water stage. The rating curve ($Q = 3.925\ H^{2.44}$, $R^2 = 0.94$; Fig 4) was then used to generate continuous discharge values from stage measurements recorded every 5 min throughout the season.~~-~~ These data were in turn averaged to yield a continuous record of hourly discharge data for 62 days, from 13 June to 13 August 2016 (Fig. 5a)~~(Fig. 4)~~.

~~Therefore, we conclude that our rating curve is sufficiently robust to estimate discharge.~~ Four uncertainty estimates were calculated as percentage uncertainties at 95% confidence interval (see Appendix A for more details): 1) uncertainty for the 46 discrete~~individual~~ discharge measurements (Ume), 2) uncertainty due to the rating curve (URC), 3) uncertainty of daily mean discharge (Xdm), and 4) uncertainty due to the stream bed incision into the ice over the melt~~ing~~ season (Uin). While ~~the uncertainty due to measurement errors (U_{me})~~ Ume was estimated at~~as~~ 10.8%, ~~uncertainty due to the rating curve (~~U_{RC}~~)~~ was estimated at 17% (Appendix A). The measurement uncertainties were encompassed in the envelope of uncertainty due to the rating curve (Q±U_{RC}) (Fig. 4). The averaging of hourly discharge to daily mean discharge generated an uncertainty of 25% (X_{dm}). ~~Uncertainty due to the stream bed incision was estimated using the cross-sectional profiles of the stream bed (Fig. 3).~~

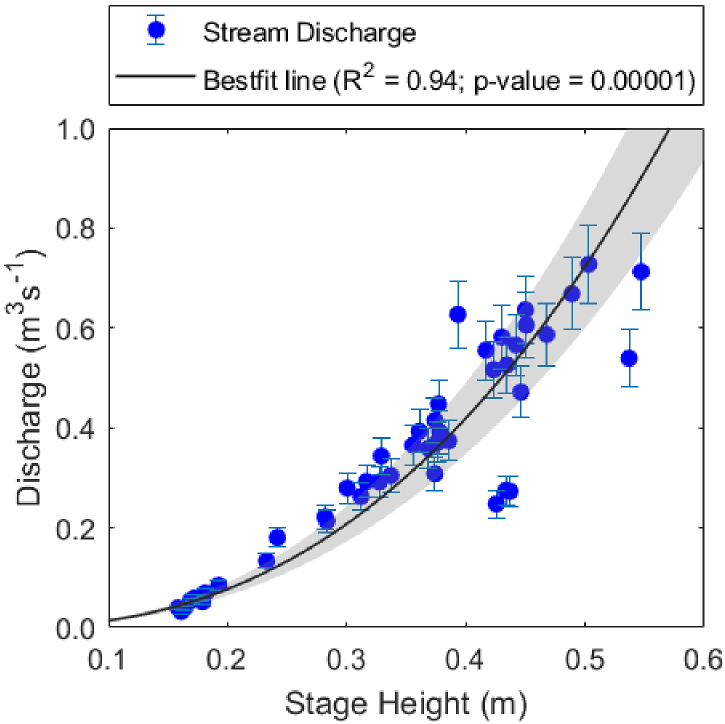

Figure 4: Rating curve (black line) determined from the best fit of power law (Eq. 1) to observations of stage and discharge (blue dots). Error bars show measurement error uncertainty (U_{me}). Rating curve uncertainty (U_{RC}) is shown in the grey shaded area (see Appendix A for uncertainty calculations).

Finally, uncertainty due to the stream bed incision was estimated using the cross-sectional profiles of the stream bed (Fig. 3). Reconstructing hydrographs for supraglacial streams with high seasonal and diurnal variations with a rating curve is typically unreliable (Smith et al., 2017, 2021; Pitcher et al., 2019). In terrestrial rivers, shifts in the rating curve are a reflection of either a datum adjustment or changes in channel cross-section. Unlike terrestrial rivers, the bed under supraglacial streams is constantly melting and incising into the ice resulting in an ever-changing cross-sectional profile. This melting may or may not alter the geometry of the stream cross section. To examine if our rating curve is robust despite channel cross-sectional profiles changes, we compared coincident depth profiles ~~collected while~~ velocity measurements~~was measured~~ (Fig. 3). The discrete discharge measurements over a cross-section are susceptible to both measurement and incision errors. However, assuming that negligible incision occurs over the 26-hour-period, uncertainty in hourly discharge measurements could be attributed to measurement errors alone. Therefore, ~~B~~by separating profiles collected over high flows through the season from profiles collected over the 26-hr period of hourly measurements~~ and assuming small incision over the 26-hour-period~~, ~~depth~~ measurement errors can be isolated from incision errors. While profiles collected over the season show a 3.7 cm standard deviation (Fig 3a), hourly profiles collected over the 26-hr period show a 1.9 cm standard deviation (Fig 3b). The uncertainty in stream discharge (here we use the 95% confidence interval) due to non-uniform stream bed incision and depth measurement errors, U_{in} is 10.9~~-~~% (of the average stream depth), and the depth measurement alone is 5.9 %. Despite these errors, the channel geometry incises uniformly through the season with all the cross-sections lying inside the uncertainty levels (Fig. 3a). Therefore, we conclude that our rating curve is sufficiently robust to estimate discharge.

3.2 Water level in the weathering crust from a cryoconite hole

Storage of melt water in the weathering crust is investigated by measuring water level in a cryoconite hole using a Levelogger®, similar to the one used to measure water level in the stream (Solinst, 2020). The Levelogger® was placed at the bottom of the cryoconite hole, for a 3-week period from 24 July to 13 August, located in the 660 catchment close to the station where discharge measurements were collected. A Barologger® was also placed at the location for barometric pressure correction of the water level.

3.3~~2~~ Calculation of hydraulic geometry parameters

At-a-station ~~H~~hydraulic geometry parameters were calculated to examine the relative importance of width, velocity, and depth in controlling discharge, and to compare with other studies reporting hydraulic geometry data for supraglacial streams. The ~~H~~hydraulic geometry ~~is a set of equations that describes the relationship between discharge and stream channel geometry, namely, width, depth, and velocity~~ power-law equations are (Leopold and Maddock, 1953):

$$w = aQ^b \tag{2}$$

$$d = cQ^f \tag{3}$$

$$v = kQ^m \tag{4}$$

where, w, d, and v are stream width, depth, and velocity of the cross-section, respectively. The exponents b, f, and m represent the slopes of the power law equations. The magnitude of the exponents represents the rates of change of each variable with respect to the independent variable, discharge Q. The coefficients a, c, and k represent the y-axis intercepts. The law of conservation of mass implies that the product of coefficients (a, c, and k) ~~should equal unity. Likewise,~~ and the sum of the exponents (b, f, and m) should ~~also~~ equal ~~unity~~one (Leopold and Maddock, 1953).

3.4~~3~~ Automatic weather station observations in the 660 catchment

~~To identify the timing of daily maximum melt during clear sky days, a shortwave pyranometer (HOBO S-LIB-M003) was mounted at 2 m height on an automated weather station (AWS) ~20–25 m from the gauging station. Other meteorological data were measured at this station and are a part of the dataset accompanying this paper. However, better data~~

~~from the HOBO station was not used in this study since better data continuity and accuracy is provided by the nearby AWS, KAN_L, located ~7–8 km southeast of our study area at 670 m elevation. Therefore, meteorological data from KAN_L were used in our analysis. The KAN_L AWS is maintained by the Geological Survey of Denmark and Greenland (GEUS) (van As et al., 2011).~~ To identify the timing of daily maximum melt during clear sky days, meteorological observations were obtained from the nearby AWS, KAN_L (van As et al., 2011) maintained by the Geological Survey of Denmark and Greenland (GEUS), located ~7–8 km southeast of our study area at 670 m elevation. We also installed a shortwave pyranometer (HOBO S-LIB-M003) at 2 m height ~20–25 m from the gauging station, but these data were not used in this study since KAN_L offered better data continuity and measurements of other surface energy components.

3.5~~4~~ Surface energy balance model

To examine surface energy drivers of supraglacial discharge, energy balance components were obtained from a surface energy balance model (described in van As, 2011). This model uses forcing data from in-situ meteorological and radiative observations from KAN_L to calculate ~~the~~ surface energy balance components net shortwave radiation, net longwave radiation, sensible heat flux, latent heat flux, sub-surface conductive heat flux, and heat flux from rain. While incoming shortwave and longwave radiation are gathered from the AWS, turbulent heat fluxes are calculated from near-surface gradients of meteorological variables, air temperature, humidity, and wind speed using Monin-Obukhov similarity theory (van As, 2011).

3.6~~5~~ Catchment delineation

The catchment boundary and supraglacial stream network were manually digitized using two sources (Fig. 1). Firstly, we used WorldView-1 (WV1) panchromatic imagery (spatial resolution of 1 m) acquired on 16 August 2016 to manually digitize the stream network. We also collected 20,000 handheld GPS points of the catchment boundary in the field, by walking along the visually-determined catchment divide ~~separating the stream network from adjacent catchments~~ on 15 August 2016. We did not observe a change in catchment size during the study period. We estimate the catchment area to be accurate within 5% (0.03 km2) given that it was manually identified in the field. However, the precise delineation of the catchment is not relevant to the outcome of the study.

4 Results

Our catchment has a dendritic drainage pattern (Strahler order = 4, as determined from our manual digitization), and is internally drained, meaning that all surface meltwater is routed through streams, tributaries, and ponds to a terminal moulin (Fig. 1). Repeated visits~~-~~ to the study site during melt season suggested that the majority of streams re-occupied existing channel networks between 2015~~3~~–2019, ~~suggest that this network, with streams~~ resulting in channels ~ 0.1–15 m wide~~ths~~ and ~ 0.1–2 m deep~~pths~~. ~~, is an annually recurrent feature of the local hydrological system. A new tributary joining the network was observed in 2017 but does not affect the present study.~~

4.1 Hourly and daily variations in supraglacial discharge

Stream discharges between 13 June and 13 August vary~~ies~~ strongly both diurnally and seasonally (Fig. 5a). Hourly discharge fell as low as 0.002 m^3s^{-1} at night and daily peaks exceeded 0.3 m^3s^{-1} on most days. Three distinct melt episodes with larger discharges were recorded on 13 June (0.81 m^3s^{-1}), 19 June (0.94 m^3s^{-1}), and 16 July (0.93 m^3s^{-1}). T~~During t~~hese ~~times~~ peak flows occurred around 15:00 local time and were almost double the seasonal~~long-term~~ average of daily maximum discharge (0.5 m^3s^{-1})~~and occurred around 15:00 local time~~. The timing of these melt episodes corresponds with periods of anomalous high river discharge observed ~35 km downstream in the Watson River, Kangerlussuaq (van As et al., 2018).

Daily maximum discharge varies from 0.05–0.94 m^3s^{-1} through the season, with the highest values around the three melt episodes (Fig. 5b). Daily minimum discharge has much less seasonal variability than daily maximum discharge but exhibits two occurrences with anomalously larger flow on 23 June and 19 July (Fig. 5b). During the melt episodes, these positive anomalies in daily minimum discharge follow a steep decrease in daily maximum discharge, meaning, the anomalously large low flows at night follow a dip in day-time streamflow.~~Compared to the first and second episodes, daily minimum discharge behaves differently after the third episode. After the second episode, and before the third episode begins,~~ Between the second and third melt episodes, night-time low-flow discharge occasionally falls as low as 0.002 m^3s^{-1} but remains above~~rises to~~ 0.04 m^3s^{-1} after the third episode. Finally, the diurnal amplitude (daily maximum minus daily minimum discharge) tracks daily maximum discharge except for the second and third melt episodes, due to~~with~~ large daily minimum discharge at those times (Fig. 5c). After the third melt episode, there is a steady decline in diurnal amplitude from 0.64 m3s-1 21 July to 0.33 m3s-1 on 13 August~~0.64–0.33 m^3s^{-1} (21 July–13 August)~~.

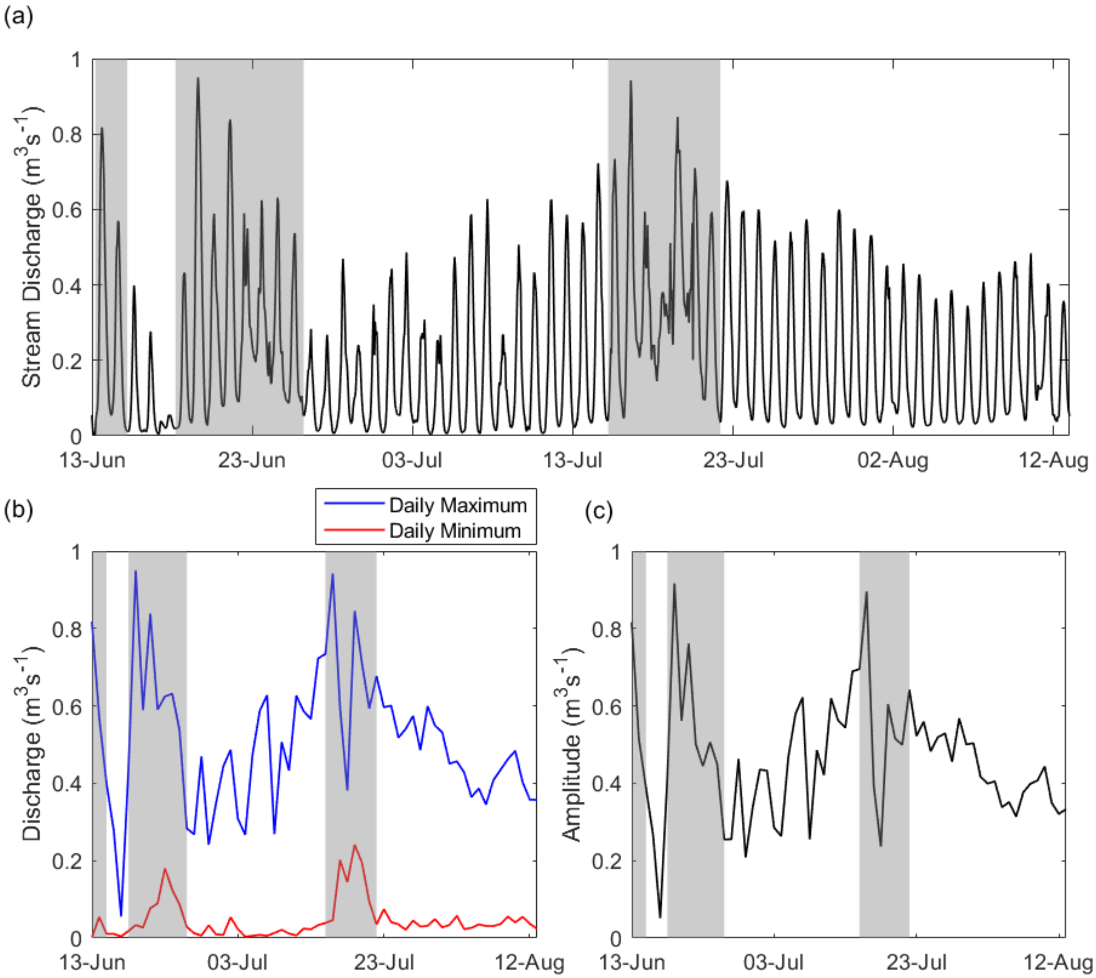
(a)
Stream Discharge ($m^3 s^{-1}$)
13-Jun
23-Jun
03-Jul
13-Jul
23-Jul
02-Aug
12-Aug
(b)
Daily Maximum
Daily Minimum
Discharge ($m^3 s^{-1}$)
(c)
Amplitude ($m^3 s^{-1}$)

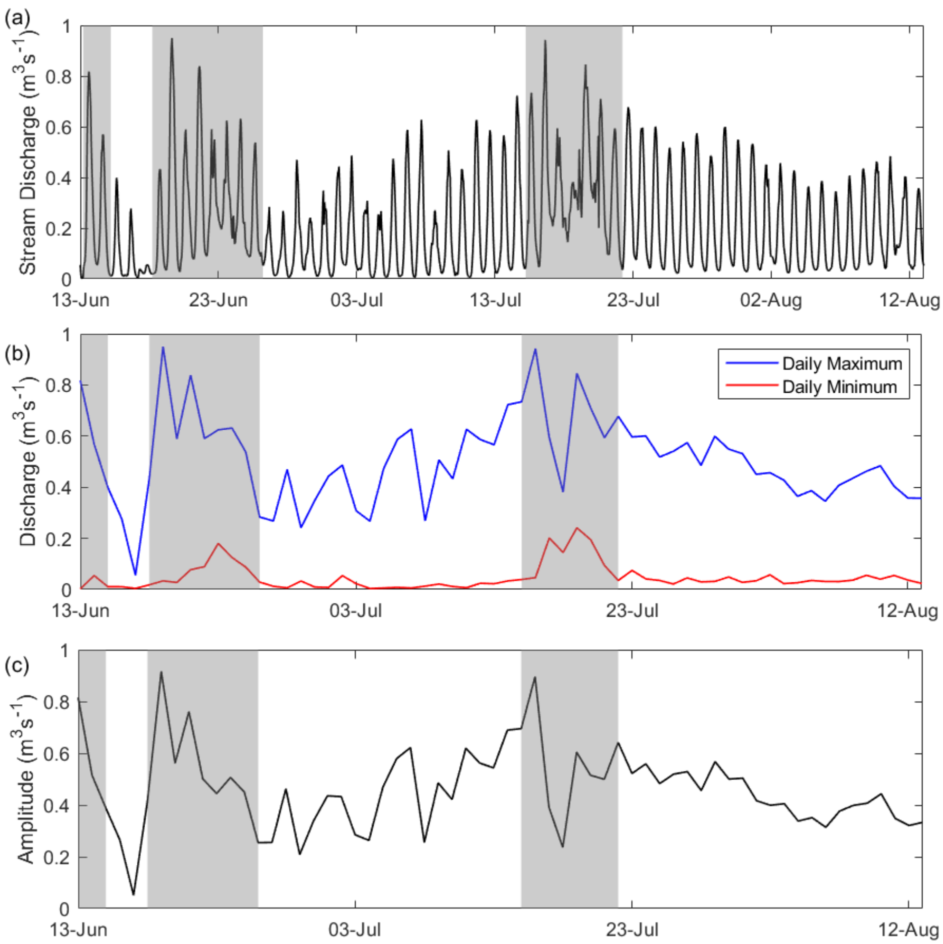

Figure 5: (a) Hourly stream discharge generated using the rating curve (Fig. 4) over 62 days of the melt~~ing~~ season. (b) Daily maximum (in blue) and daily minimum (in red) discharge, calculated from the hourly discharge. (c) Amplitude (daily maximum minus daily minimum) of the stream discharge. Three large melt episodes are shown in grey shaded regions.

The daily mean discharge varies from 0.02–0.51 m^3s^{-1} over the 62 days (Fig. 6a) and co-varies seasonally with daily maximum discharge except during the second and third melt episodes ~~for the timing of the peak daily mean discharge~~ (Fig. 5b). The daily mean discharge peaks on 19 July, three days after the second-largest melt episode in hourly discharge. In contrast, the second largest peak in daily mean flow occurs on 20 June, which is the same day as the largest episode in hourly discharge. In both cases, hourly maximum discharge is accompanied by several days of very high daily minimum flows (Fig. 5b), which explains the discrepancy between the timing of the daily mean and daily maximum episodes.

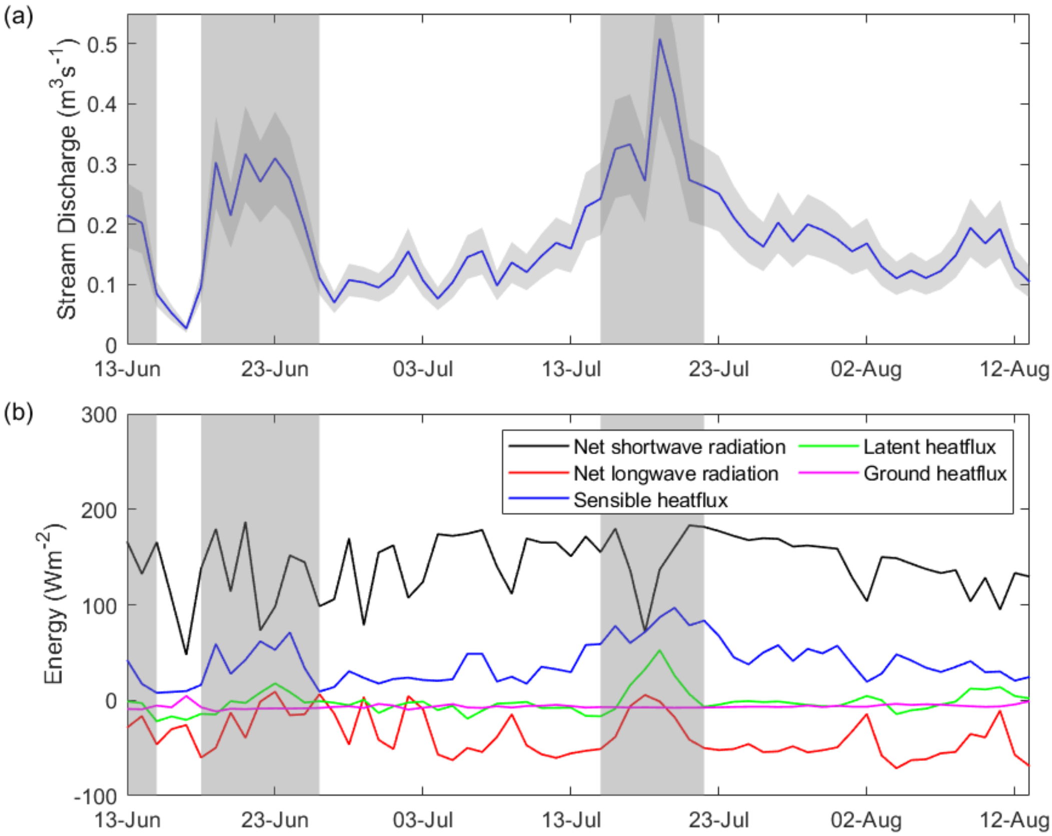

Figure 6:(a) Daily discharge measured by averaging the hourly discharge from Fig. 5a. Uncertainty of daily mean discharge generated by averaging hourly discharge, X_{dm}, is shown in the grey shaded area (see Appendix A for uncertainty calculations), (b) surface energy components, net shortwave radiation (black), net longwave radiation (red), sensible heat flux (blue), latent heat flux (green), and ground heat flux (magenta). Large melt episodes are shown in grey shaded regions.

4.2 Surface energy balance

Throughout the season, net shortwave radiation exceeds all other surface energy fluxes and thus is the primary driver of stream discharge (Fig. 6b). However, the second and third melt episodes coincide with peak longwave radiation (65 Wm^{-2} increase compared to before the episodes) and turbulent heat fluxes (40–80 Wm^{-2} increase) along with a drop in shortwave radiation (110–120 Wm^{-2} decrease) (Fig. 6). Thus, during high-melt episodes, longwave radiation and turbulent heat fluxes become more pronounced drivers of streamflow. Among all energy fluxes, sensible heat flux correlates most with daily mean discharge (R=0.88, p-value ≤~~=~~ 0.~~000~~01). During the third melt episode, the hourly peak discharge coincides with a peak in shortwave radiation on 16 July (Fig. 7a). However, the peak daily mean discharge occurs three days later on 19 July 2016 due to high net longwave radiation and turbulent heat fluxes from 16–20 July (Fig. 6). This high net longwave radiation was caused by overcast conditions (with cloud cover consistently greater than 0.4, except for a couple of hours throughout a 96-hour period; Fig. 7b) and resulted in a large~~high~~ low~~-~~ flow at night (Fig. 7a). The consistently large low-flow persisted from 17 to

20 July (Fig. 7a) and resulted in the seasonal peak discharge on 19 July (0.51 m^3s^{-1}) (Fig. 6a). This can also be seen in the hourly variation of surface energy balance components and stream discharge (Fig. 7a). Between 17–20 July, night-time streamflow is much higher than before and after the third melt episode (Fig. 7a), and coincides with increased net longwave radiation. While a dip in shortwave radiation on 18 July decreases the high flow during the day, the low flow during the night increases due to a spike in net longwave radiation (Fig. 7a)~~.~~

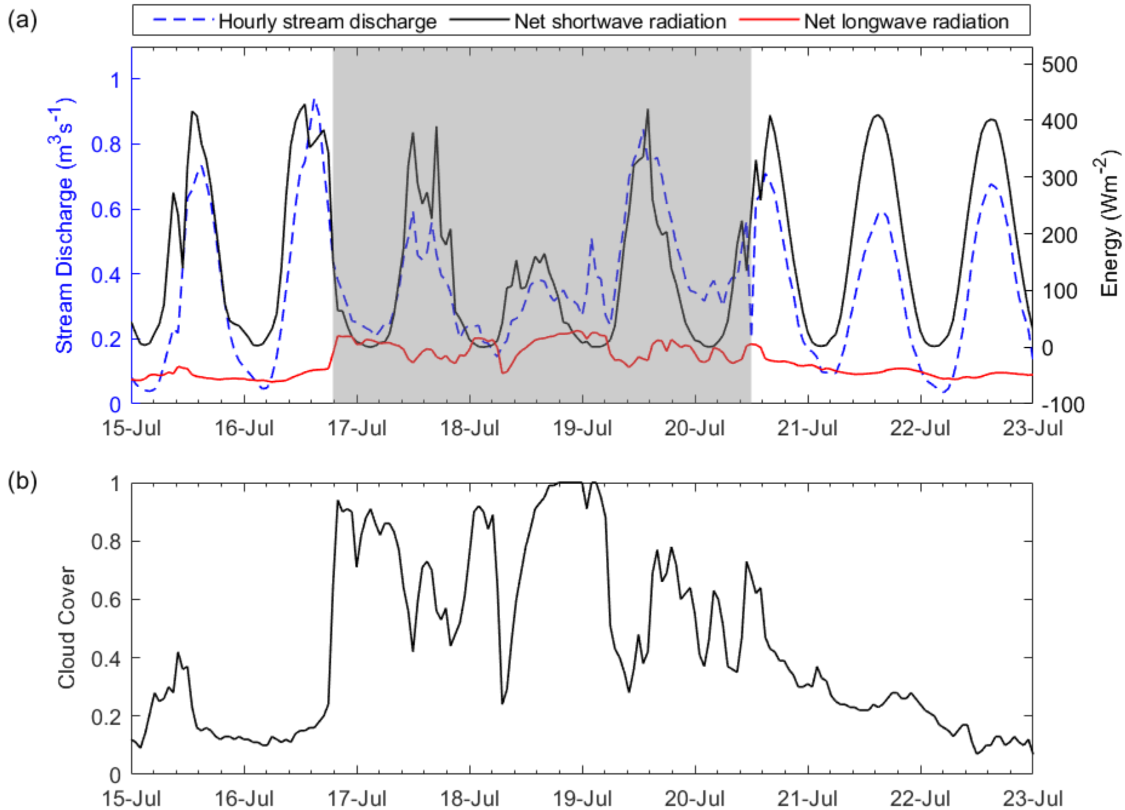
(a)
Hourly stream discharge
Net shortwave radiation
Net longwave radiation
Stream Discharge (m^{3}s^{-1})
Energy (Wm^{-2})
1
0.8
0.6
0.4
0.2
0
500
400
300
200
100
0
-100
15-Jul
16-Jul
17-Jul
18-Jul
19-Jul
20-Jul
21-Jul
22-Jul
23-Jul
(b)
Cloud Cover
1
0.8
0.6
0.4
0.2
0
15-Jul
16-Jul
17-Jul
18-Jul
19-Jul
20-Jul
21-Jul
22-Jul
23-Jul

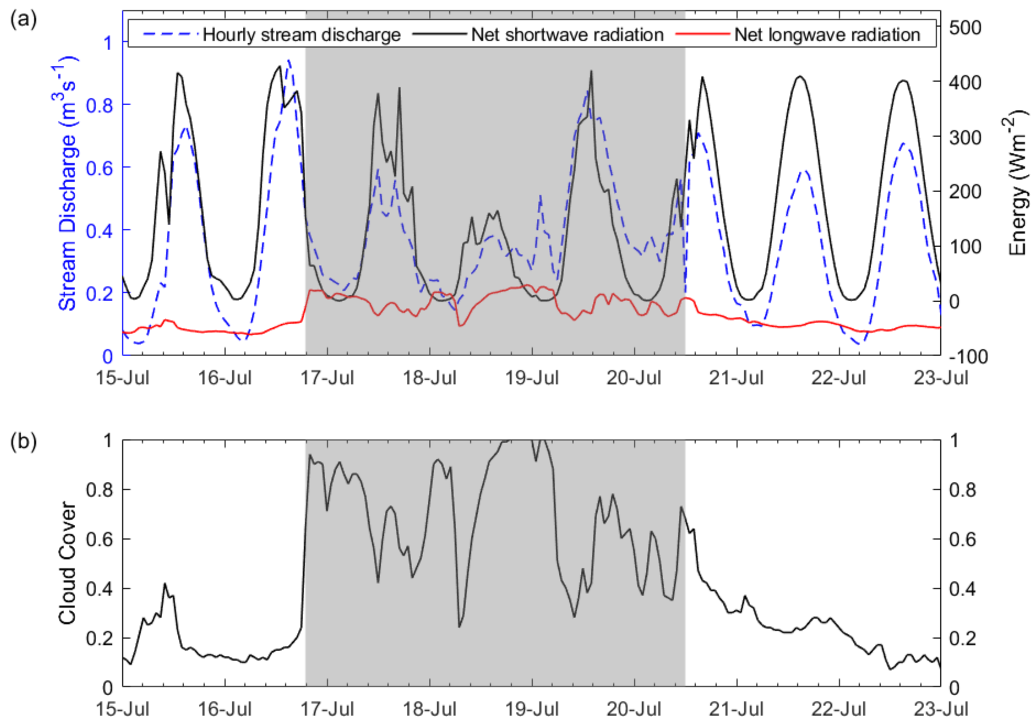

Figure 7: (a) Diurnal fluctuations in stream discharge on the left y-axis (blue dotted line) and surface energy balance components on the right y-axis, net shortwave radiation in black, and net longwave radiation in red from 15–22 July. (b) Cloud cover at the KAN_L station from 15–22 July. The large daily minimum period (a subset of the third melt episode) with cloud cover consistently greater than 0.4, except for a couple of hours throughout a 96-hour period, is shown in the grey shaded region. ~~(b) Cloud cover at the KAN L station from 15–22 July.~~

To further examine each~~the difference in~~ energy balance components' contribution to ~~high versus low~~ stream discharge, we aggregated components for the second and third melt episodes, and compared them to ~~all-season~~ data spanning the entire melt season (Fig. 8). Contribution of individual components is estimated as a ratio to the total melt energy and is described as the proportion of melt energy. The shortwave radiation proportion of melt energy fell by 40% from a melt proportion of 1.13 to 0.73~~from 78 % to 50 % (normalized)~~ during the melt episodes. Simultaneously, the contribution of longwave radiation and turbulent heat fluxes increased during those days. The longwave radiation's proportion of melt energy increased from a melt season~~al~~ average of -0.32 to -0.08~~5~~ during the peak flow days~~ (increased by 16.5%)~~, corresponding to an increase in contribution by 24% (Fig. 8). ~~while s~~Sensible and latent heat fluxes' proportion of melt energy increased~~ by 0.06 (4%) and 0.11 (7%)~~ from 0.28 to 0.34 (6%) and from -0.4 to 0.6 (10%) during the melt episodes, respectively (Fig. 8).

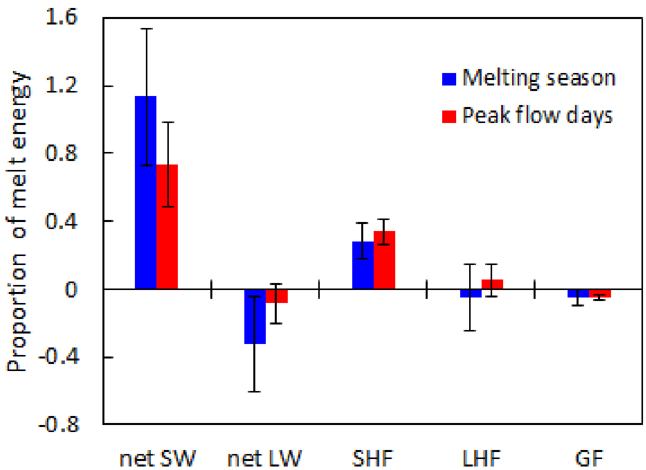

Figure 8: Proportion of melt energy (ratio of each component to total melt energy) for the whole melt~~ing~~ season in blue and for the days during the melt episodes only in red. Here, peak flow days include days from the second melt episode (19–23 June) and the third melt episode (16–20 July). Error bars represent standard deviation of each sample. net SW - net shortwave radiation, netLW - net longwave radiation, SHF - sensible heat flux, LHF - latent heat flux, GF - ground heat flux.

4.3 Timing of ~~peak~~ daily maximum discharge

To examine if the transport of meltwater from its production on the ice sheet surface to the discharge observation site varies over the season, we calculated time to daily maximum discharge, following 'time-to-peak' methodology in traditional terrestrial hydrology (Chow, 1964). As the season progresses, the timing~~e to~~ of daily maximum discharge will reflect temporary changes in ~~network~~melt storage within the weathering crust and meltwater transport efficiency. In contrast, during clear-sky days, when solar radiation drives melt, the timing of daily maximum surface meltwater production~~creation~~ is not expected to change over the season and is~~be~~ proportional to solar noon. Therefore, during the clear sky days, variability in timing of daily maximum discharge can be attributed to network storage and transport efficiency as opposed to non-clear sky days with noise in the signal due to the variation in incoming solar radiation and clouds (Fig. S2). For example, when cloud cover greater than 60% persisted for longer than 3–4 hours during the middle of the day (10:00–16:00 local time), peak discharge occurs earlier in the day, around noon to 13:00 local time. However, if cloud cover persists less than 3 hours around mid-day, peak discharge occurs later in the day between 15:00–17:00 local time.

While the incoming solar radiation peaks at solar noon (around 13:15 local time), the timing of the daily maximum discharge varies from 16:00 in late June to 14:00 in late July (Fig. 9a). In other words, ~~T~~the peak time lag between the solar and discharge peaks changes from 3 hours to 1 hour from 30 June to 31 July and has a statistically significant negative trend (R^2 = 0.793, p-value <= 0.01~~0.00011~~). After 31 July, the peak time lag abruptly shifts back to early melt season conditions of a ~~initial season conditions and stabilizes at~~ 3-~~-~~hour~~s in early August~~ peak time lag. This shift in the peak time lag coincides with the sudden decrease in daily mean temperatures from 4.3 °C on 31 July to 2.5 °C on 3 August~~-~~, with daily minimum temperatures dropping down to 1 °C (Fig. 9b). ~~Though the daily mean temperature started to decrease after the third melt~~

~~episode on 19 July, the sudden drop in early August coincides with the shift in time of daily maximum discharge due to a drop in night-time temperatures close to 1 °C (Fig. 9b).~~ These air temperature measurements were collected at 2 m above the surface and therefore the skin temperatures are expected to be below freezing causing meltwater delivery to the channels to slow down. With below freezing temperatures, there is likely an increase in Manning's n coefficient (i.e. quantifies channel roughness and friction; Chow, 1964) as frozen ice features pose an impedance to flow, in turn lowering the streams' conveyance. In addition to the change in temperature, a sudden drop in water level in the weathering crust cryoconite hole coincides with the drop in temperature and abrupt shift in time of daily maximum discharge (Fig. 9c). A steep change in the cryoconite hole water level is seen during early August, at the same time as shift in time of peak discharge and a drop in temperature.

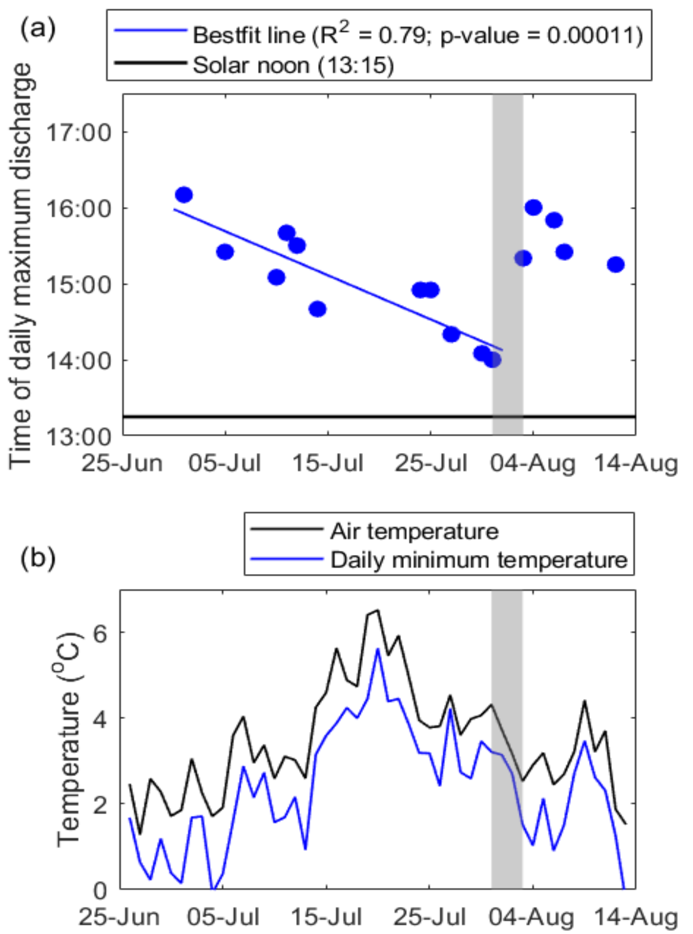

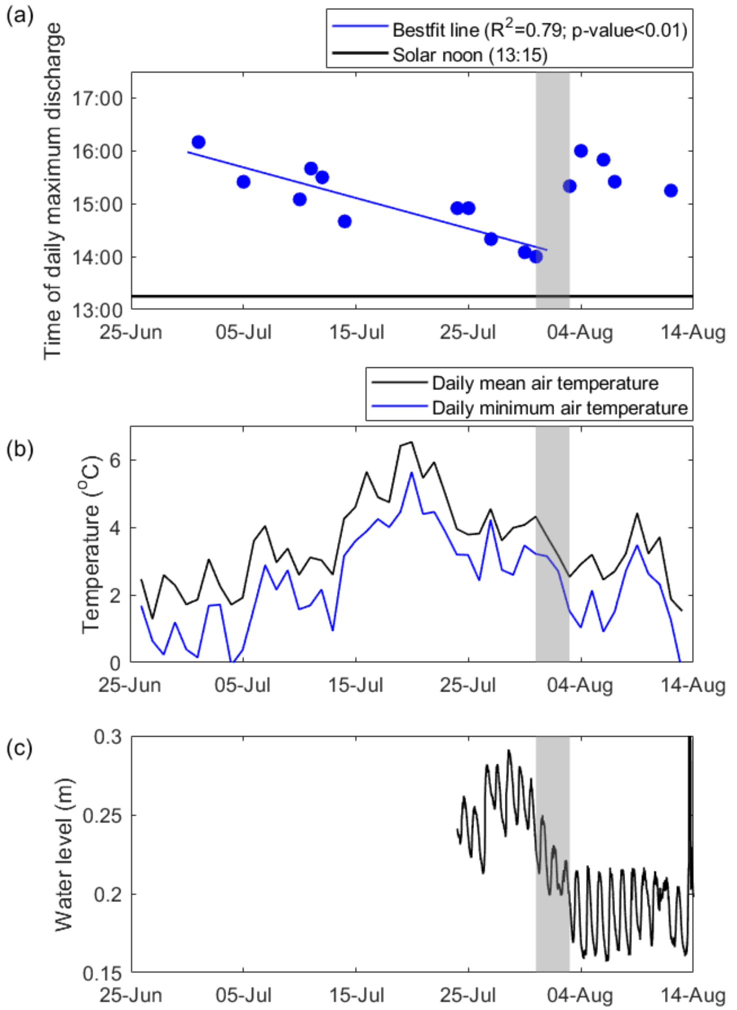

Figure 9: (a) Time to daily maximum discharge for clear sky days. Clear sky days were identified as days with incoming solar radiation (from KAN_L AWS data) with a smooth diurnal cycle and lacking short-term, hourly, fluctuations from varying cloud cover. (b) Daily mean air temperature from KAN_L AWS. The period, where change in time of daily maximum discharge coincides with a sudden drop in temperature from 1–3 Aug, is shown in the grey shaded region. (c) Water level in a cryoconite hole in the weathering crust. Measurements were made with the same type of Solinst Levelogger® as used to measure channel water level.

4.4 Hydraulic Geometry

Hydraulic geometry parameters are determined by generating a power law between stream discharge, and width (R^2 = 0.87, p-value $<$ 0.01~~= 0.00001~~), depth (R^2 = 0.94, p-value $<$ 0.01~~= 0.00001~~) and velocity (R^2 = 0.88, p-value $<$ 0.01~~= 0.00001~~) (Eq. 2–4 respectively). For the 660 catchment, the exponents b, f, and m are 0.194, 0.387 and 0.373 respectively, and coefficients a, c, and k are 3.44, 0.541, and 0.632 respectively. In theory ~~While~~ the sum of the exponents of these power laws, representing sensitivity of discharge to the individual variable, equals 1, and the product of the coefficients must also equal 1 (Leopold and Maddock, 1953). But, in practice, due to measurement error and when R2<1.0, i.e., the power law does not perfectly describe the data, and we can expect deviations from 1. In our study the sum of exponents equals 0.95 and the product of coefficients equals 1.17.

Variation in hydraulic geometry parameters was investigated over three time periods of the melt season, 17 June–20 July, 26–27 July and 4 August. Though these time periods have different sample sizes (N = 15, 27 and 4 respectively), the R2 values for all the parameters are greater than 0.89 (p-value < 0.01) for both before and after melt episode. However, the parameters in the August sample are not significant with R2 values 0.51, 0.52 and 0.01 (p-value equal to 0.25, 0.32 and, 0.96) for width, depth and velocity exponents respectively due to a small sample size. Analysis over different time periods of the melt season show a dramatic drop in the velocity exponent (m) on 4 August compared to earlier in the season (Fig. 10). Velocity had a higher exponent (meaning stronger relation to Q), compared to other parameters until early August, which shifts to depth having stronger relation to Q, thereby reducing the dependency of Q on velocity. While the width exponent (b) ranges between 0.1–0.2 throughout the season, the depth exponent increases gradually from 0.3 before the July melt episode to 0.4 after the melt episode to 0.5 in early August.

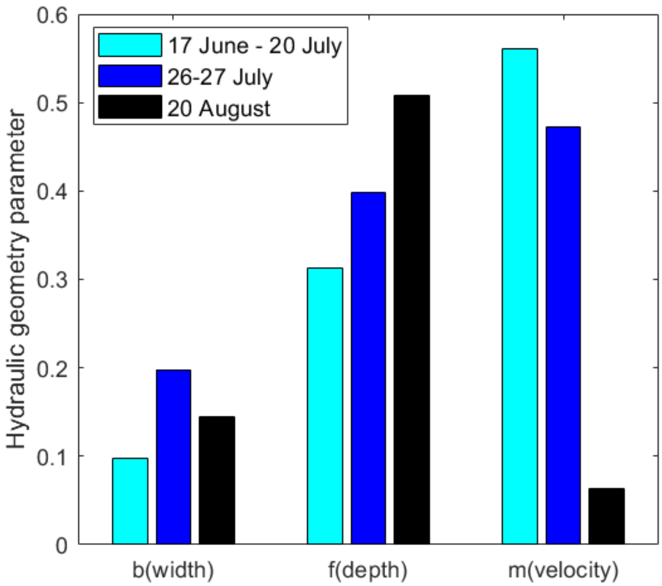

Figure 10: Hydraulic geometry parameters calculated for three different times, 1) bulk of melt season before peak (melt episode in July), 2) after the peak (melt episode in July), but before increase in peak timing, 3) after the peak (melt episode in July), and after increase in peak timing (in early August).

5 Discussion

Here, we present a 62-day time-series of supraglacial stream discharge (13 June–13 August 2016). We find strong diurnal variability in stream discharge, similar to previous in situ studies of supraglacial streamflow (Holmes, 1955; Knighton, 1981; Marston, 1983; Mernild et al., 2006; McGrath et al., 2011; Chandler et al., 2013; Wadham et al., 2016;

Smith et al., 2017, 2021; Chandler et al., 2021), despite different locations. At our study site, the 660 catchment (0.6±0.03 km2) ~~D~~diurnal variability ranges from close to zero to ~~0.002~~ 0.95 m^3s^{-1} with daily maximum discharge occurring between 14:00–16:00 local time throughout the study period. Both diurnal variability and time of maximum discharge are comparable to McGrath et al. (2011), wh~~o~~ich documented diurnal variability of 0.017–0.54 m^3s^{-1} with a daily maximum discharge at 16:45 local time over a catchment (in Sermeq Avannarleq ablation zone in central-west Greenland) of area 1.14±0.06 km^2 from 3–17 August 2009 (Table 1). Marston (1983) also finds a similar range of discharge varying between close to zero to~~0–~~ 0.23 m^3s^{-1} with a daily maximum discharge occurring between 14:00–16:00 local time on the~~in~~ Juneau Icefield around late July. Mernild et al. (2006) and Chandler et al. (2013) show a larger catchment~~, over southeast and southwest Greenland respectively, with~~ reports a diurnal variability up to 10 times larger than at the 660 catchment and a daily maximum discharge occurring between 14:00–18:00 local time from two catchments larger than the 660 catchment. The oldest study we are aware of, Holmes (1955), reports supraglacial stream discharge of 0.14–5 m^3s^{-1} (about five times larger than at the 660 catchment) at a catchment of 25–50 km^2(~~much~~40–80 times larger than the 660 catchment) with a daily maximum discharge occurring between 16:00–20:00 local time in southwest Greenland. In an even larger catchment (60-63 km2, ~100 times larger than the 600 catchment), ~~study by~~ Smith et al. (2017 and 2021) ~~in a much larger (63 km²) supraglacial catchment,~~ document that the daily maximum discharge occurred between 18:00–20:00 and 20:30–22:40 local time, and discharge varied between 4.6~~5~~-26.7 m^3s^{-1} and 5.8–37.6 m3s-1(Table 1). Synthesizing ~~In~~ all studies providing time-series of stream discharge (Marston, 1983; Mernild et al., 2006; McGrath et al., 2011; Chandler et al., 2013; Smith et al., 2017, 2021), the lag between solar noon and daily maximum discharge, i.e., the peak time lag, ~~between solar noon and daily maximum discharge~~ is larger for the larger magnitude of stream discharge.~~, due to runoff generation from a larger catchment area, thus increasing the distance of surface routing and a later peak of daily discharge at the catchment outlet~~ This can be explained by the fact that when runoff is generated over a larger catchment area, the distance of surface routing increases and thus delays daily maximum discharge at the catchment outlet (Yang and Smith, 2016; Smith et al., 2017; King 2018).

~~In addition to the diurnal variability, supraglacial stream discharge exhibits strong seasonal variability at the 660 catchment. We observed three melt episodes of high discharge, one peaking on 13 June (350% of mean discharge), a second on 19 June (400% of mean discharge), and a third on 16 July (400% of mean discharge) (Fig. 5a). The timing of these episodes corresponds with periods of anomalous high river discharge observed ~35 km downstream in the Watson River, Kangerlussuaq (van As et al., 2018). The 660 catchment is a very small subcatchment of the Watson River catchment (12000 km²).~~

Over the 62-day study period, while net shortwave radiation provides the majority of melt energy and is the primary driver of streamflow, net longwave radiation and turbulent heat fluxes (sensible and latent) become more dominant melt drivers during the three melt episodes (Fig. 8). These findings disagree with studies suggesting that overcast conditions, resulting in lower solar radiation, reduce surface melt in the ablation zone (Hofer et al., 2017; Izeboud et al., 2020) but agree with Greenland-wide studies identifying a link between longwave radiation and enhanced surface melting (Van Tricht et al., 2016; Gallagher et al., 2020)~~ while disagreeing with studies suggesting that overcast conditions and lower solar radiation reduce~~

~~surface melt in the ablation zone (Hofer et al., 2017; Izeboud et al., 2020)~~. Furthermore, out of all energy balance components (e.g. net shortwave radiation, R2=0.23, p-value=0.035), the~~we find that~~ daily average sensible heat flux has the highest correlation with stream discharge (R^2=0.83, p-value < 0.01~~=0.00001~~)~~ of all energy balance components (e.g. net shortwave radiation, R^2=0.23, p-value=0.035)~~. ~~Correlating energy components with stream discharge without a time lag is justified here due to the quick routing in this catchment (1–3 hours).~~ This contribution of sensible heat flux is consistent with Fausto et al. (2016), who show that peak melting occurs at times with anomalously large turbulent energy fluxes. Correlating energy components with stream discharge without a time lag is justified here due to the quick routing in this catchment (1–3 hours). Though previous studies have shown a similar link between sensible heat flux and episodes of intense melting (van As et al., 2012; Fausto et al. 2016; Wang et al., 2021), all of them rely on model simulated melt using local weather station data while we are using stream discharge in this study. Net shortwave radiation has the largest contribution to total meltwater production which is reduced by 40% (melt proportion decreases from 1.13 to 0.73) during the melt episodes. This reduction in contribution to melt is compensated by net longwave radiation, sensible and latent heat fluxes which increased by 24%, 6% and 10% (corresponding to melt proportion increase from -0.032 to -0.08, 0.28 to 0.34, and -0.4 to 0.6) respectively during the melt episodes.

Table 1: Table of measured supraglacial streamflow, width and catchment size from this and previous studies. "Width" denotes stream width and "Lag" is the time of peak discharge after solar noon.

Source	Location	Time	Discharge ($m^3 s^{-1}$)	Width (m)	Catchment Area (km^2)	Lag (hours)
Holmes et al. (1955)	Alpha River, Project Mint Julep, southwest Greenland	21 July – 15 August, 1953	~0.14 – 5.11	9	25 – 50	3 – 7
Knighton (1981)	Austre Okstindbreen, Norway	NA	0.005 – 0.02	0.2 – 0.5	NA	NA
Marston (1983)	Juneau Icefield	28 July – 2 August, 1983	~0 – 0.24**	0.7 – 1.6	NA	2 – 3
Mernild et al. (2006)	Mittivakkat Glacier, southeast Greenland	16 – 19 August 2004, 15 – 18 June 2005	5 – 10	NA	18.4	3 – 4 (August) 5 – 7 (May)
McGrath et al. (2011)	West Greenland	3 – 17 August, 2009	0.017 – 0.54	0 – 2.5	1.14 ± 0.06	3 – 4
Chandler et al. (2013)	Moulin L41 – internally drained catchment (part of Leverett catchment), southwest Greenland	29 June – 7 July 17 – 20 August, 2011	~0.1 – 8**	NA	NA	3 – 6 (July) 6 – 8 (August)

Wadham et al. (2016)	Leverett Glacier, southwest Greenland	16 June – 10 August	~0 – 12**	NA	NA	NA
Gleason et al. (2016), (& Smith et al., 2015)*	Southwest Greenland	July – August, 2012	0.006 – 0.402 (small streams) 4.58 – 23.12 (large streams)	0.2 – 3.84 (small streams) 7.19 – 20.62 (large streams)	NA	NA
Smith et al. (2017)	Southwest Greenland	20 – 23 July, 2015	4.61 – 26.73	6 – 19~~2.4 ± 1.5~~	63.1	4 – 6
Smith et al. (2021)	Southwest Greenland	6 – 13 July, 2016	5.75 – 37.61	up to ~30 (est.)	60.2	6.5 – 7.5
660 Catchment	Southwest Greenland	13 June – 13 August, 2016	0.002~~1~~ – 0.95	1.6 – 3.2	0.6	1 – 3

* Smith et al. (2015) and Gleason et al. (2016) have common data sets. Range of width and discharge are the same for both the studies. However, Gleason et al. (2016) primarily discussed the hydraulics of these streams. Therefore, this data set is mentioned as Gleason et al. (2016) in the discussion.
** Discharge from these studies is visually estimated from their figures and therefore approximated to the closest first decimal place. The lower bound of stream discharge in Marston (1983) is taken as zero as the value was very small and close to zero in the figure presented.

~~We find that the time of maximum diurnal discharge varies from 16:00 in late June to 14:00 in late July (Fig. 9a), which translates to a lag between maximum diurnal melt and maximum diurnal discharge from 1–3 hours. This lag is consistent with the previous studies, where it varies from 3–9.5 hours (Holmes, 1955; Mernild et al., 2006; McGrath et al., 2011; Chandler et al., 2013; Smith et al., 2017). The difference in lag is most likely due to the difference in the size of catchment. While large catchments in Holmes (1955), Mernild et al. (2006), Chandler et al. (2013) and Smith et al. (2017) show lags between 3–9.5 hours, smaller catchments in Marston (1983) and McGrath et al. (2011) show lags between 2–4 hours (Table 1). For the 660 catchment, the lag decreases through the season from 3 hours in late June to 1 hour in late July, consistent with the change in lag through the melting season shown by Mernild et al. (2006) from 5–7 hours in May to 3–4 hours in August. Furthermore, at the 660 catchment, in early August, the lag abruptly increases to the initial season conditions and stabilizes at 3 hours, coinciding with a sudden drop in air temperature from 4.3 °C to 2.5 °C from 31 July to 3 August (Fig. 9b). With the night-time air temperatures close to 1 °C, the skin temperatures could be below freezing affecting the efficiency of the stream network, thereby increasing the temporary storage of melt generated in the weathering crust, and delay the transport of melt to the moulin. This phenomenon of a shift in the timing of daily maximum discharge agrees with the model study by Yang et al. (2018), who shows that a poorly developed stream network has delayed timing of peak and up to half the diurnal variation in stream discharge relative to a well-developed and an efficient network.~~

For the 660 catchment, the lag between peak incoming solar radiation and daily maximum discharge decreases through the season from 3 hours in late June to 1 hour in late July. The shorter peak time lag compared to previous studies (3-9.5 hours, Holmes, 1955; Mernild et al., 2006; McGrath et al., 2011; Chandler et al., 2013; Smith et al., 2017) is likely due to the smaller size of the 660 catchment. The reduced lag time through the melt season is consistent with the change observed by Mernild et al. (2006) from 5–7 hours in May to 3–4 hours in August attributed to changes in the structure of the weathering crust. Furthermore, at the 660 catchment, in early August, the peak time lag abruptly increases to the initial season conditions and stabilizes at 3 hours, coinciding with a sudden drop in air temperature from 4.3 °C to 2.5 °C from 31 July to 3 August (Fig. 9b). The time of daily maximum discharge is driven by the catchement's ability to evacuate water which in turn depends on the rate of melt water transport in the stream channels and the proportion of the transport distance that is dictated by porous media flow (i.e. non-channelized flow through the weather crust and over bare ice). Melt water trapped in the weathering crust also can decrease drainage efficiency. This drainage efficiency depends on the geometry of the channel network, the hydraulic conductivity and storage capacity of the weathering crust, and the frictional coefficient of the streambed (Karlstrom, 2014; Gleason et al., 2015; Cooper et al., 2018). We hypothesize that, as the season progresses to peak discharge in July and melt water production increases, the catchment increases the proportion of channelized flow compared to porous media flow as demonstrated in a modeling study, Yang et al. (2018). Increased importance of channelized flow results in an increase in the drainage efficiency and earlier time of peak discharge. The high melt episodes with increased longwave radiation also contribute to the drainage efficiency by decreasing the storage capacity (Takeuchi, 2000). However, in early August, a steep drop in water level inside the weathering crust coincides with a drop in air temperature. With the night-time air temperatures close to 0°C, the streambed likely partially freezes. This ice formation impedes flow, likely causing an increase in the Manning's n coefficient of the stream channel. This in turn causes discharge to be more regulated by changes in cross sectional area rather than in velocity, which is seen as a sharp drop in m (velocity exponent) in early August (Fig. 10). This also likely coincides with the stream network switching back to a higher proportion of porous media flow, which by definition have longer transport distances and therefore will increase the peak time lag. Additionally, similar to the stream bed, the weathering crust is likely at freezing temperatures in August, which thus results in increased interstitial freezing and decrease in hydraulic conductivity.

Our work confirms the findings by Gleason et al. (2016) that hydraulic geometry parameters cannot be generalized for supraglacial rivers in Greenland, despite having a common ice substrate. This study furthers Gleason's conclusions by analyzing streams closer to the ice edge showing that hydraulic parameters are still highly spatially and temporally variable across the ice sheet and may vary over a melt season. Comparing our data with parameters from previous studies (Knighton, 1981; Marston, 1983; Gleason et al., 2016) in a ternary diagram reveals three clusters (Fig. 11~~0~~). These three clusters can be grouped based on their b-values (width ~~power-law~~ exponent). The first cluster has high b-values (b>=0.35) and includes the downstream station of Gleason et al. (2016), which are smaller streams with discharge varying between 0.006 to 0.402 m^3s^{-1}. The second cluster has low b-values (b<=0.05) and includes at-a-station data from Gleason et al. (2016), which are larger streams with discharge varying between 4.58 to 23.12 m^3s^{-1}. Finally, the third cluster has moderate b-values (0.05<b<0.35), and includes this study, and Knighton (1981) and Marston (1983). Though the discharge from Knighton (1981) is two orders smaller than ours, Marston (1983) has similar discharge values (Table 1). The streams with discharge of same order of magnitude i.e., varying between 0–1 $m^3 s^{-1}$, from Knighton (1981), Marston (1983), and the current study show moderate sensitivity to stream width (moderate values of b) and streams with higher magnitude of discharge show very small sensitivity to stream width (smaller values of b). However, small streams from Gleason et al. (2016) do not concur with this generalization and show a high sensitivity to stream width (large b-values). Changing hydraulic geometry parameters over the melt season may explain some of the differences between the studies, as our parameters determined during the main melt season (17 June to 20 July) are close to large streams parameters from Gleason et al. (2016) which were collected in mid-late July. On the other hand, our parameters determined at the end of the melt season (4 August) approaches small stream parameters from Gleason et al. (2016) which were collected around mid-August. These parameters seem to be more dependent on the time of the melt season than the location or size of the streams.

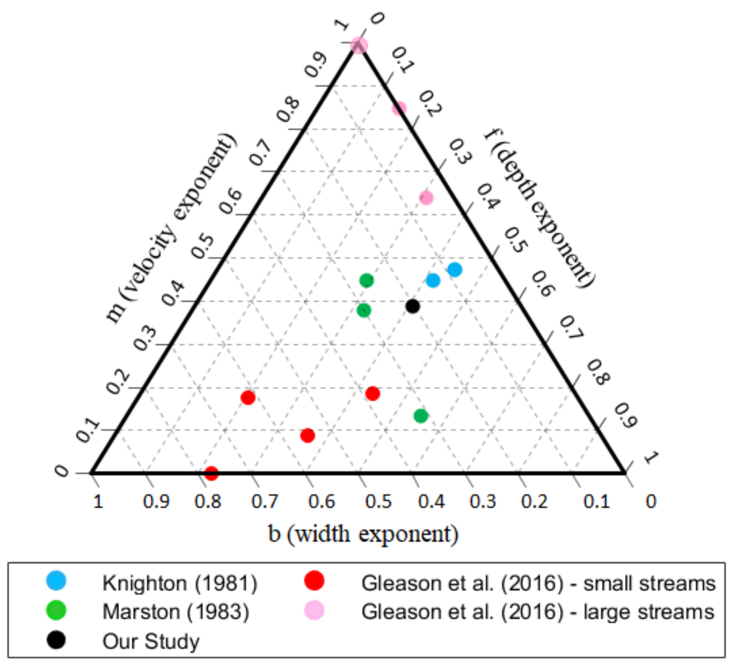

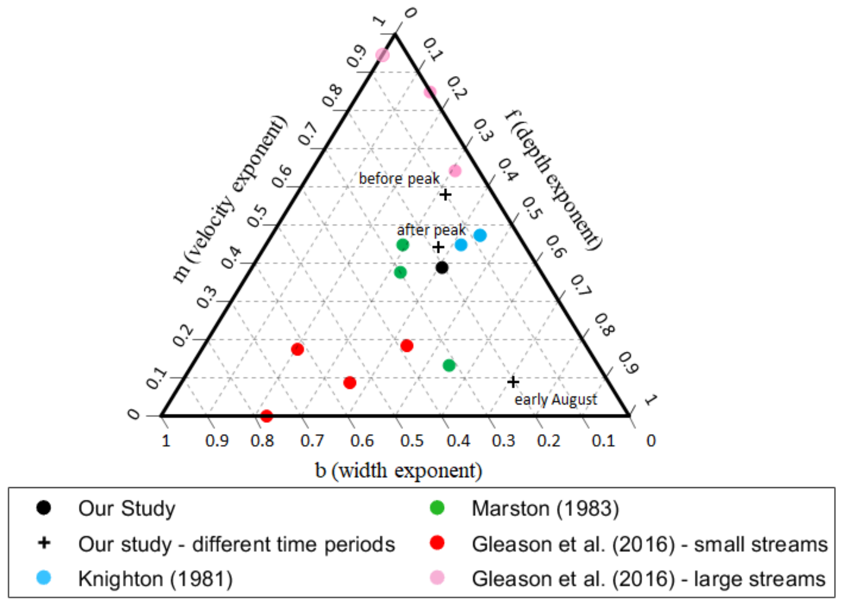

Figure 11~~0~~: Ternary diagram comparing m, f, and b parameters from this study (in black; whole season in solid dot, different time periods in '+' with before peak - 17 June–20 July, after peak - 26–27 July, and early August - 4 August) with previous work by Knighton (1981) in blue, Marston (1983) in green, and Gleason et al. (2016) large streams in pink and small streams in red. Where m+f+b exceeded unity, parameters were adjusted to unity.

Our analysis of a season-long record of streamflow and its drivers has several implications for large-scale Greenland ice sheet hydrology. First, we ~~confirm Gleason et al. (2016)'s work by finding that hydraulic geometry parameters vary across ice sheet catchments. Thus, using generalized parameter space to estimate supraglacial streamflow from ungauged catchments may not be valid. Second, we~~ find that longwave radiation and turbulent fluxes have an increased contribution by 24% and 16% respectively ~~(adding up to 50% of melt energy)~~, in governing stream discharge during the melt episodes. Given that several regional climate models underestimate turbulent fluxes, they also will underestimate melt episodes (van den Broeke et al., 2011; and Fausto et al., 2016). Since one of the most widely used methods~~the most accurate way~~ to estimate surface runoff from the entire Greenland ice sheet is through regional climate/surface mass balance models (Cullather et al., 2016; Fettweis et al., 2017; Mernild et al., 2018; Noel et al., 2018), underestimating turbulent heat fluxes also underestimates runoff. Second~~Third~~, with the lack of long-term~~lengthy~~ records of supraglacial stream discharge over the Greenland ice sheet, the 62-day long time series could expand climate/surface mass balance models validation capability ~~to a great extent~~. For context~~Currently~~, a recent~~the only~~ study ~~to~~ validating~~e~~ model simulated runoff using~~ed~~ field observations of streamflow covers~~ing~~ just 3 days (Smith et al. 2017). Lastly, understanding the evolution of~~the~~ accurate timing and magnitude of peak discharge throughout the melt season may aid ~~can be helpful in~~ future studies about ~~understand~~ its influence on subglacial water pressure and ice velocities. ~~However, this study couldn't investigate that influence, although~~ ~~as the impact of stream velocities~~ on subglacial water pressure is ~~are probably minor from this catchment since it is located very close to the ice sheet margin.~~

6 Conclusions

We present one of the longest records of Greenland supraglacial stream discharge, spanning 62-days of the 2016 melt~~ing~~ season for a 0.6 km^2 catchment in southwest Greenland. These ~~long-term~~ observations could be used in validating regional climate models, currently the best tools to estimate surface runoff from the entire Greenland ice sheet. ~~Concurring with the previous studies, we show that hydraulic geometry parameters cannot be generalized for supraglacial rivers in Greenland.~~ The observed stream discharges vary both seasonally and diurnally. Our record includes three distinct episodes of large discharge, one from 13–14 June, a~~the~~ second ~~one~~ from 19–25 June, and a~~the~~ third ~~one~~ from 15–21 July. The daily maximum discharge and amplitude show similar seasonal and diurnal variations except during the second and third melt episodes when nighttime melting reduced the daily amplitude. During the third melt episode, the large daily discharge minimums drive~~minimums, caused by high longwave radiation, drive~~ the seasonal peak discharge on 19 July with continuous high flow in the day and night for 3–4 days (16–19 July). The stream discharge is primarily driven by net shortwave radiation through the melt~~ing~~ season, except during the high melt episodes when net longwave radiation and turbulent heat fluxes show an increased contribution (24~~16~~% and ~~4–7~~16% respectively) to melt energy. The lag between the time of daily maximum discharge and time of daily maximum melt (~~assumed to be~~ i.e., solar noon ~~here~~) varies through the season from 3 hours in late June to 1 hour in late July and goes back to 3 hours in early August. The abrupt shift in peak time lag in early August is attributed to a sudden drop in air temperature, steep decrease in temporary water storage in the weathering crust, and a change in hydraulic geometry ~~due to a sudden drop in air temperature~~. The~~is~~ change in peak time lag through the season could be due to the expansion and contraction of the stream network, caused by probable freezing skin temperatures at night, affecting network efficiency and therefore, change in routing time of the melt. Though this theory was explained by a model simulation from Yang et al. (2018), further work is required to reveal if the rapid shift in the timing of peak discharge, which we ~~notice~~observe at the 660 catchment, also takes place across Greenland supraglacial streams, over larger catchments and at higher elevations compared to our study and to analyze the influence of stream network development on timing and magnitude of peak discharge.

Appendix A: Streamflow uncertainty

The uncertainty of the 46 individual discharge observations due to seven different types of measurement errors in velocity and stage height was calculated following Herschy (2002) and WMO (2010), and assumes that segment discharges and standard uncertainties are approximately equal in each of the segments in the cross-section:

$$U_{me}(Q) = K\sqrt{u_m^2 + u_s^2 + \frac{1}{M}\left\{u_b^2 + u_d^2 + u_p^2 + u_c^2 + u_e^2\right\}} \quad \text{(A1)}$$

where U_{me} is uncertainty due to measurement errors, Q is discharge, K is the so called coverage factor (K=2 gives the 95% confidence interval), u_m is uncertainty in determination of mean velocity for number of verticals (M), u_s is uncertainty due to calibration errors, u_b is uncertainty in width, u_d is uncertainty in depth, u_p is uncertainty in determination of mean velocity for number of points in the vertical, u_c is uncertainty in determination of mean velocity for current meter rating, and u_e is uncertainty in determination of mean velocity for time of exposure. A summary of all nomenclature used in this study is found in Table A1.

Table A1: Nomenclature used in this paper

Symbol	Unit	Description
H	m	Water level/Stage height
Q	m^3s^{-1}	Discharge
Q_i	m^3s^{-1}	Measured stream discharge
Q_c	m^3s^{-1}	Estimated stream discharge from a rating curve
w	m	Width
d	m	Depth
v	ms^{-1}	Velocity
α	m	Datum correction (stage at zero flow)
β	-	Constant (exponent in the rating curve equation)
p	-	Constant (coefficient multiplying stage in the rating curve equation)
a	-	Width hydraulic geometry coefficient
c	-	Depth hydraulic geometry coefficient
k	-	Velocity hydraulic geometry coefficient
b	-	Width hydraulic geometry exponent
f	-	Depth hydraulic geometry exponent
m	-	Velocity hydraulic geometry exponent
N	-	number of data points in a sample
n	-	number of discharge measurements
M	-	number of verticals
K	-	coverage factor (k=2 for 95% C.I)
t	-	Student’s t correction (for 95% confidence t=2)
u_m	%	Uncertainty in determination of mean velocity for number of verticals
u_s	%	Uncertainty due to calibration errors
u_b	%	Uncertainty in width
u_d	%	Uncertainty in depth
u_p	%	Uncertainty in determination of mean velocity for number of points in the vertical
u_c	%	Uncertainty in determination of mean velocity for current meter rating
u_e	%	Uncertainty in determination of mean velocity for time of exposure
U_{RC}	%	Uncertainty of hourly stream discharge due to the rating curve
U_{me}	%	uncertainty due to measurement errors
U_{in}	%	uncertainty due to streambed incision
X_{dm}	%	uncertainty in the daily mean discharge
S_e	%	standard error of estimate
S_{mr}	%	standard error of mean
S_{wl}	%	standard error of log of water level measurement

Using Equation A1 and literature values for the seven measurement errors (Table A2), we find U_{me} = 10.8%.

The uncertainty in hourly stream discharge due to the rating curve was determined with a statistical method by calculating the standard error of estimate, S_e, where the quadratic rating curve was linearized with a logarithmic transformation following Herschy (1994):

$$S_e = \pm t\sqrt{\frac{\sum_{i=1}^{n} \quad (lnQ_i - lnQ_c)^2}{n-2}} \qquad \text{(A2)}$$

where t is Student's t correction (for 95% confidence t=2), n is number of discharge measurements, Q_i is discharge measured, and Q_c is discharge estimated using a rating curve.

Table A2: Standard uncertainties in a single measurement of stream discharge due to seven measurement errors, using empirical values from WMO (2010). Final uncertainty due to measurement error is calculated with 95% CI using the empirical values from this table. Please refer to Table A1 for Nomenclature.

Uncertainties	Values used in this study
u_m	4.5 % for a minimum of 10 verticals
u_s	1 %
u_b	0.15 % (for width range 0 – 100 m)
u_d	0.65 % (for depth range 0.4 – 6 m)
u_p	7.5 % (number of verticals = 1)
u_c	1 % (for average velocity of around 0.25 ms^{-1}
u_e	4% (for time of exposure between 30 – 60 s)
M	10 (number of verticals varied between 10-16
K	2 for 95% C.I

Using Equation A2, the uncertainty of hourly stream discharge due to the rating curve, U_{RC} is calculated to 17%.

Lastly, the uncertainty in daily mean discharge due to the averaging of hourly data is estimated in two steps using the methodology of Dymond and Christain (1982). First, S_{mr}, the standard error of the daily mean, is calculated using a logarithmic transformation of discharge, Q from Equation 1, in order to make it a linear relation:

$$S_{mr} = \pm t S_e \left(\frac{1}{N} + \frac{(lnln\ (h+\alpha) - \underline{ln(h+\alpha)})^2}{\sum \quad (lnln\ (h+\alpha) - \underline{ln(h+\alpha)})^2} \right)^{1/2} \qquad \text{(A3)}$$

where, N is the number of data points in the sample (here, 24 samples in a day). Second, X_{dm} is uncertainty in the daily mean discharge is calculated as:

$$X_{dm} = \frac{1}{N} \sum_{i=1}^{N} \quad \sqrt{S_{mr}^2 + \beta^2 S_{wl}^2}\ Q_i \qquad \text{(A4)}$$

where, S_{wl} is the standard error of log of water level measurement (calculated using Equation A2). Using Equation A3 and A4, the uncertainty in the daily mean discharge, X_{dm} is calculated to 25 %. All uncertainties are expressed as the 95% confidence level.

Author contribution statement

RM performed data analysis and wrote the manuscript with support from AR. RM and AR conceived and planned the study. SL and MC did the majority of field data collection, with support from RM, AR, and SC. DvA performed surface energy balance modeling. All authors discussed the results and contributed to the final manuscript.

Acknowledgements

~~We are thankful for the support of Polar Field Services and the Rutgers Geography Department.~~ Funding for this work comes from the NASA Cryosphere program (Award# 80NSSC19K0942 and #NNX14AH93G) managed by Dr. Thorsten Markus. SL was funded by the NSF Graduate Research Fellowship Program. QGIS was used to prepare maps. Polar Geospatial Center's Arctic DEMs were used in this study. We are thankful for the support of Polar Field Services and the Rutgers Geography Department. We ~~T~~thank ~~you to~~ Kyle Mattingly, Jing Xiao, ~~and~~ Isatis Cintron, David Chandler, and three anonymous reviewers for constructive feedback on the manuscript.

Data availability

KAN_L weather station data from the Programme for Monitoring of the Greenland Ice Sheet (PROMICE) and the Greenland Analogue Project (GAP) were provided by the Geological Survey of Denmark and Greenland (GEUS) at http://www.promice.dk. All other data will be available at the PANGEA repository (in the meanwhile this data is made available to the reviewers as supplementary material).

Competing interests

The authors declare that they have no conflicts of interest.

References

Andreadis, K. M., Brinkerhoff, C. B. and Gleason, C. J.: Constraining the assimilation of SWOT observations with hydraulic geometry relations, Water Resour. Res., 56(5), 1–21, doi:10.1029/2019WR026611, 2020.

Andrews, L. C., Catania, G. A., Hoffman, M. J., Gulley, J. D., Lüthi, M. P., Ryser, C., Hawley, R. L. and Neumann, T. A.: Direct observations of evolving subglacial drainage beneath the Greenland Ice Sheet, Nature, 514(7520), 80–83, doi:10.1038/nature13796, 2014.

Ashmore, P. and Sauks, E.: Prediction of discharge from water surface width in a braided river with implications for at-a-station hydraulic geometry, Water Resour. Res., 42(3), 1–11, doi:10.1029/2005WR003993, 2006.

Bartholomew, I., Nienow, P., Sole, A., Mair, D., Cowton, T. and King, M. A.: Short-term variability in Greenland Ice Sheet motion forced by time-varying meltwater drainage: Implications for the relationship between subglacial drainage system behavior and ice velocity, J. Geophys. Res. Earth Surf., 117, 1–17, doi:10.1029/2011JF002220, 2012.

~~Bell, R. E., Chu, W., Kingslake, J., Das, I., Tedesco, M., Tinto, K. J., Zappa, C. J., Frezzotti, M., Boghosian, A. and Lee, W. S.: Antarctic ice shelf potentially stabilized by export of meltwater in surface river, Nature, 544(7650), 344 348, doi:10.1038/nature22048, 2017.~~

Bennartz, R., Shupe, M. D., Turner, D. D., Walden, V. P., Steffen, K., Cox, C. J., Kulie, M. S., Miller, N. B. and Pettersen, C.: July 2012 Greenland melt extent enhanced by low-level liquid clouds, Nature, 496(7443), 83–86, doi:10.1038/nature12002, 2013.

Chandler, D. M., Wadham, J. L., Lis, G. P., Cowton, T., Sole, A., Bartholomew, I., Telling, J., Nienow, P., Bagshaw, E. B., Mair, D., Vinen, S. and Hubbard, A.: Evolution of the subglacial drainage system beneath the Greenland Ice Sheet revealed by tracers, Nat. Geosci., 6(3), 195–198, doi:10.1038/ngeo1737, 2013.

Chandler, D. M., Wadham, J. L., Nienow, P. W., Doyle, S. H., Tedstone, A. J., Telling, J., Hawkings, J., Alcock, J. D., Linhoff, B. and Hubbard, A.: Rapid development and persistence of efficient subglacial drainage under 900 m-thick ice in Greenland, Earth Planet. Sci. Lett., 566, 116982, doi:10.1016/j.epsl.2021.116982, 2021.

Chen, X., Zhang, X., Church, J. A., Watson, C. S., King, M. A., Monselesan, D., Legresy, B. and Harig, C.: The increasing rate of global mean sea-level rise during 1993 – 2014, Nat. Clim. Chang., 7(July), 492–495, doi:10.1038/nclimate3325, 2017.

Chow, V. T.: Handbook of Applied Hydrology: A Compendium of Water-Resources Technology, McGraw-Hill Company, New York., 1964.

Chu, V. W.: Greenland ice sheet hydrology: A review, Prog. Phys. Geogr., 38(1), 19–54, 2014.

Colgan, W., Steffen, K., McLamb, W. S., Abdalati, W., Rajaram, H., Motyka, R., Phillips, T. and Anderson, R.: An increase in crevasse extent, West Greenland: Hydrologic implications, Geophys. Res. Lett., 38(18), 1–7, doi:10.1029/2011GL048491, 2011.

Cook, J. M., Hodson, A. J. and Irvine-Fynn, T. D. L.: Supraglacial weathering crust dynamics inferred from cryoconite hole hydrology, Hydrol. Process., 30(3), 433–446, doi:10.1002/hyp.10602, 2016.

Cooper, M. G., Smith, L. C., Rennermalm, A. K., Mige, C., Pitcher, L. H., Ryan, J. C., Yang, K. and Cooley, S. W.: Meltwater storage in low-density near-surface bare ice in the Greenland ice sheet ablation zone, Cryosphere, 12(3), 955–970, doi:10.5194/tc-12-955-2018, 2018.

Cullather, R. I., Nowicki, S. M. J., Zhao, B. and Koenig, L. S.: A characterization of Greenland ice sheet surface melt and runoff in contemporary reanalyses and a regional climate model, Front. Earth Sci., 4, 1–20, doi:10.3389/feart.2016.00010, 2016.

Das, S. B., Joughin, I., Behn, M. D., Howat, I. M., King, M. A., Lizarralde, D. and Bhatia, M. P.: Fracture propagation to the base of the Greenland ice sheet during supraglacial lake drainage, Science, 320(5877), 778–781, doi:10.1126/science.1153360, 2008.

Dymond, J. R. and Christian, R.: Accuracy of discharge determined from a rating curve, Hydrol. Sci. J., 27(4), 493–504, doi:10.1080/02626668209491128, 1982.

Fausto, R. S., van As, D., Box, J. E., Colgan, W., Langen, P. L. and Mottram, R. H.: The implication of nonradiative energy fluxes dominating Greenland ice sheet exceptional ablation area surface melt in 2012, Geophys. Res. Lett., 43, 2649–2658, doi:10.1002/2016GL067720, 2016.~~Fausto, R. S.: The implication of nonradiative energy fluxes dominating Greenland ice sheet exceptional ablation area surface melt in 2012, Geophys. Res. Lett., 43, 2649–2658, doi:10.1002/2016GL067720, 2016.~~

Ferguson, R. I.: Hydraulics and hydraulic geometry, Prog. Phys. Geogr., 10, 1–31, 1986.

Fettweis, X., Box, J. E., Agosta, C., Amory, C., Kittel, C., Lang, C., Van As, D., Machguth, H. and Gallée, H.: Reconstructions of the 1900-2015 Greenland ice sheet surface mass balance using the regional climate MAR model, Cryosphere, 11(2), 1015–1033, doi:10.5194/tc-11-1015-2017, 2017.

Flowers, G. E.: Hydrology and the future of the Greenland Ice Sheet, Nat. Commun., 9(1), 1–4, doi:10.1038/s41467-018-05002-0, 2018.

Gallagher, M. R., Chepfer, H., Shupe, M. D. and Guzman, R.: Warm temperature extremes across Greenland connected to clouds, Geophys. Res. Lett., 47(9), 1–10, doi:10.1029/2019GL086059, 2020.

Gardner, A. S., Moholdt, G., Scambos, T., Fahnstock, M., Ligtenberg, S., Van Den Broeke, M. and Nilsson, J.: Increased West Antarctic and unchanged East Antarctic ice discharge over the last 7 years, Cryosphere, 12(2), 521–547, doi:10.5194/tc-12-521-2018, 2018.

Gardner AS, Fahnestock MA, Scambos TA. ITS_LIVE regional glacier and ice sheet surface velocities. Data archived at National Snow and Ice Data Center, 2019.

Gleason, C. J.: Hydraulic geometry of natural rivers: A review and future directions, Prog. Phys. Geogr., 39(3), 337–360, doi:10.1177/0309133314567584, 2015.

Gleason, C. J., Smith, L. C., Chu, V. W., Legleiter, C. J., Pitcher, L. H., Overstreet, B. T., Rennermalm, A. K., Forster, R. R. and Yang, K.: Characterizing supraglacial meltwater channel hydraulics on the Greenland Ice Sheet from in situ observations, Earth Surf. Process. Landforms, 41(14), 2111–2122, doi:10.1002/esp.3977, 2016.

Herschy, R. W.: The uncertainty in a current meter measurement, Flow Meas. Instrum., 13(5–6), 281–284, doi:10.1016/S0955-5986(02)00047-X, 2002.

Herschy, R.: The stage-discharge relation, Flow Meas. Instrum., 4(1), 11–15, 1993.

Herschy, R.: The velocity-area method, Flow Meas. Instrum., 4(1), 7–10, doi:10.1016/0955-5986(93)90004-3, 1993.

Herschy, R.: The analysis of uncertainties in the stage-discharge relation, Flow Meas. Instrum., 5(3), 188–190, doi:10.1016/0955-5986(94)90018-3, 1994.

Hewitt, I. J.: Seasonal changes in ice sheet motion due to melt water lubrication, Earth Planet. Sci. Lett., 371–372, 16–25, doi:10.1016/j.epsl.2013.04.022, 2013.

Hofer, S., Tedstone, A. J., Fettweis, X. and Bamber, J. L.: Decreasing cloud cover drives the recent mass loss on the Greenland Ice Sheet, Sci. Adv., 3(6), doi:10.1126/sciadv.1700584, 2017.

Hoffman, M. J., Catania, G. A., Neumann, T. A., Andrews, L. C. and Rumrill, J. A.: Links between acceleration, melting, and supraglacial lake drainage of the western Greenland Ice Sheet, J. Geophys. Res. Earth Surf., 116(4), 1–16, doi:10.1029/2010JF001934, 2011.

Holmes, G. W.: Morphology and hydrology of the Mint Julep area, southwest Greenland. In Project Mint Julep: Investigation of Smooth Ice Areas of the Greenland Ice Cap, 1953; Part II: Special Scientific Reports., 1–50, 1955.

Izeboud, M., Lhermitte, S., Van Tricht, K., Lenaerts, J. T. M., Van Lipzig, N. P. M. and Wever, N.: The spatiotemporal variability of cloud radiative effects on the Greenland Ice Sheet surface mass balance, Geophys. Res. Lett., 47(12), 1–9, doi:10.1029/2020GL087315, 2020.

Karlstrom, L., Zok, A. and Manga, M.: Near-surface permeability in a supraglacial drainage basin on the Llewellyn Glacier, Juneau Icefield, British Columbia, Cryosphere, 8(2), 537–546, doi:10.5194/tc-8-537-2014, 2014.

~~Kingslake, J., Ely, J. C., Das, I. and Bell, R. E.: Widespread movement of meltwater onto and across Antarctic ice shelves, Nature, 544(7650), 349–352, doi:10.1038/nature22049, 2017.~~

King, L.: Comparing two methods of remotely estimating moulin discharge on the Greenland ice sheet, J. Glaciol., 64(247), 850–854, doi:10.1017/jog.2018.65, 2018.

Knighton, A. D.: Channel form and flow characteristics of supraglacial streams, Austre Okstindbreen, Norway, Arct. Alp. Res., 13(3), 295, doi:10.2307/1551036, 1981.

Lampkin, D. J. and VanderBerg, J.: Supraglacial melt channel networks in the Jakobshavn Isbræ region during the 2007 melt season, Hydrol. Process., 28, 6038–6053, doi:10.1002/hyp.10085, 2014.

Leidman, S. Z., Rennermalm, Å. K., Muthyala, R., Guo, Q. and Overeem, I.: The Presence and Widespread Distribution of Dark Sediment in Greenland Ice Sheet Supraglacial Streams Implies Substantial Impact of Microbial Communities on Sediment Deposition and Albedo, Geophys. Res. Lett., 48(1), doi:10.1029/2020GL088444, 2021.

Leopold, L. and Maddock, T.: The hydraulic geometry of stream channels and some physiographic implications, US Government Printing Office., 1953.

Marston, R. A.: Supraglacial stream dynamics on the Juneau Icefield, Ann. Assoc. Am. Geogr., 73(4), 597–608, doi:10.1111/j.1467-8306.1983.tb01861.x, 1983.

Mattingly, K. S., Mote, T. L. and Fettweis, X.: Atmospheric river impacts on Greenland Ice Sheet surface mass balance, J. Geophys. Res. Atmos., 123(16), 8538–8560, doi:10.1029/2018JD028714, 2018.

McGrath, D., Colgan, W., Steffen, K., Lauffenburger, P. and Balog, J.: Assessing the summer water budget of a moulin basin in the sermeq avannarleq ablation region, Greenland ice sheet, J. Glaciol., 57(205), 954–964, doi:10.3189/002214311798043735, 2011.

Mernild, S. H., Hasholt, B. and Liston, G. E.: Water flow through Mittivakkat Glacier, Ammassalik Island, SE Greenland, Geogr. Tidsskr., 106(1), 25–43, doi:10.1080/00167223.2006.10649543, 2006.

Mernild, S. H., Liston, G. E., van As, D., Hasholt, B. and Yde, J. C.: High-resolution ice sheet surface mass-balance and spatiotemporal runoff simulations: Kangerlussuaq, west Greenland, Arctic, Antarct. Alp. Res., 50(1), doi:10.1080/15230430.2017.1415856, 2018.

Mouginot, J., Rignot, E., Bjørk, A. A., van den Broeke, M., Millan, R., Morlighem, M., Noël, B., Scheuchl, B. and Wood, M.: Forty-six years of Greenland Ice Sheet mass balance from 1972 to 2018, Proc. Natl. Acad. Sci. U. S. A., 116(19), 9239–9244, doi:10.1073/pnas.1904242116, 2019.

Moustafa, S. E., Rennermalm, A. K., Smith, L. C., Miller, M. A., Mioduszewski, J. R., Koenig, L. S., Hom, M. G. and Shuman, C. A.: Multi-modal albedo distributions in the ablation area of the southwestern Greenland Ice Sheet, Cryosphere, 9(3), 905–923, doi:10.5194/tc-9-905-2015, 2015.

Munro, D. S.: Delays of supraglacial runoff from differently defined microbasin areas on the Peyto Glacier, Hydrol. Process., 25(19), 2983–2994, doi:10.1002/hyp.8124, 2011.

Noël, B., Van De Berg, W. J., Van Wessem, J. M., Van Meijgaard, E., Van As, Di., Lenaerts, J. T. M., Lhermitte, S., Munneke, P. K., Smeets, C. J. P. P., Van Ulft, L. H., Van De Wal, R. S. W. and Van Den Broeke, M. R.: Modelling the climate and surface mass balance of polar ice sheets using RACMO2 - Part 1: Greenland (1958-2016), Cryosphere, 12(3), 811–831, doi:10.5194/tc-12-811-2018, 2018.

Pitcher, L. H. and Smith, L. C.: Supraglacial streams and rivers, Annu. Rev. Earth Planet. Sci., 421–452, doi:10.1146/annurev-earth-053018-060212, 2019.

Rennermalm, a K., Moustafa, S. E., Mioduszewski, J., Chu, V. W., Forster, R. R., Hagedorn, B., Harper, J. T., Mote, T. L., Robinson, D. a, Shuman, C. a, Smith, L. C. and Tedesco, M.: Understanding Greenland ice sheet hydrology using an integrated multi-scale approach, Environ. Res. Lett., 8(1), 015017, doi:10.1088/1748-9326/8/1/015017, 2013.

Ryan, J. C., Smith, L. C., Van As, D., Cooley, S. W., Cooper, M. G., Pitcher, L. H. and Hubbard, A.: Greenland Ice Sheet surface melt amplified by snowline migration and bare ice exposure, Sci. Adv., 5(3), 1–11, doi:10.1126/sciadv.aav3738, 2019.

Schoof, C.: Ice-sheet acceleration driven by melt supply variability, Nature, 468(7325), 803–806, doi:10.1038/nature09618, 2010.

Shepherd, A., Hubbard, A., Nienow, P., King, M. A., McMillan, M. and Joughin, I.: Greenland ice sheet motion coupled with daily melting in late summer, Geophys. Res. Lett., 36(1), 2–5, doi:10.1029/2008GL035758, 2009.

~~Shepherd, A., Ivins, E., Rignot, E., Smith, B., van den Broeke, M., Velicogna, I., Whitehouse, P., Briggs, K., Joughin, I., Krinner, G., Nowicki, S., Payne, T., Scambos, T., Schlegel, N., A, G., Agosta, C., Ahlstrøm, A., Babonis, G., Barletta, V. R., Bjørk, A. A., Blazquez, A., Bonin, J., Colgan, W., Csatho, B., Cullather, R., Engdahl, M. E., Felikson, D., Fettweis, X.,~~

~~Forsberg, R., Hogg, A. E., Gallee, H., Gardner, A., Gilbert, L., Gourmelen, N., Groh, A., Gunter, B., Hanna, E., Harig, C., Helm, V., Horvath, A., Horwath, M., Khan, S., Kjeldsen, K. K., Konrad, H., Langen, P. L., Lecavalier, B., Loomis, B., Luthcke, S., McMillan, M., Melini, D., Mernild, S., Mohajerani, Y., Moore, P., Mottram, R., Mouginot, J., Moyano, G., Muir, A., Nagler, T., Nield, G., Nilsson, J., Noël, B., Otosaka, I., Pattle, M. E., Peltier, W. R., Pie, N., Rietbroek, R., Rott, H., Sandberg Sørensen, L., Sasgen, I., Save, H., Scheuchl, B., Schrama, E., Schröder, L., Seo, K. W., Simonsen, S. B., Slater, T., Spada, G., Sutterley, T., Talpe, M., Tarasov, L., van de Berg, W. J., van der Wal, W., van Wessem, M., Vishwakarma, B. D., Wiese, D., Wilton, D., Wagner, T., Wouters, B. and Wuite, J.: Mass balance of the Greenland Ice Sheet from 1992 to 2018, Nature, 579(7798), 233–239, doi:10.1038/s41586-019-1855-2, 2019.~~

Smith, L. C., Chu, V. W., Yang, K., Gleason, C. J., Pitcher, L. H., Rennermalm, A. K., Legleiter, C. J., Behar, A. E., Overstreet, B. T., Moustafa, S. E., Tedesco, M., Forster, R. R., LeWinter, A. L., Finnegan, D. C., Sheng, Y. and Balog, J.: Efficient meltwater drainage through supraglacial streams and rivers on the southwest Greenland ice sheet, Proc. Natl. Acad. Sci., 112(4), 1001–1006, doi:10.1073/pnas.1413024112, 2015.

Smith, L. C., Yang, K., Pitcher, L. H., Overstreet, B. T., Chu, V. W., Rennermalm, Å. K., Ryan, J. C., Cooper, M. G., Gleason, C. J., Tedesco, M., Jeyaratnam, J., van As, D., van den Broeke, M. R., van de Berg, W. J., Noël, B., Langen, P. L., Cullather, R. I., Zhao, B., Willis, M. J., Hubbard, A., Box, J. E., Jenner, B. a. and Behar, A. E.: Direct measurements of meltwater runoff on the Greenland ice sheet surface, Proc. Natl. Acad. Sci., 114(50), E10622-31, doi:10.1073/pnas.1707743114, 2017.

Smith, L. C., Andrews, L. C., Pitcher, L. H., Overstreet, B. T., Rennermalm, K., Cooper, M. G., Cooley, S. W., Ryan, J. C., Miège, C., Kershner, C. and Simpson, C. E.: Supraglacial River Forcing of Subglacial Water Storage and Diurnal Ice Sheet Motion, Geophys. Res. Lett., 48(7), doi:10.1029/2020GL091418, 2021.~~Smith, L. C., Andrews, C. A., Pitcher, L. H., Overstreet, B. T., Rennermalm, Å. K., Cooper, M. G., Cooley, S. W., Ryan, J. C., Miège, C., Kershner, C., Simpson, C. E.: Supraglacial meltwater forcing of subglacial water storage and diurnal ice sheet motion, (Submitted), 2020.~~

Sole, A., Nienow, P., Bartholomew, I., Mair, D., Cowton, T., Tedstone, A. and King, M. A.: Winter motion mediates dynamic response of the Greenland Ice Sheet to warmer summers, Geophys. Res. Lett., 40(15), 3940–3944, doi:10.1002/grl.50764, 2013.

Solinst Canada Ltd.: Solinst 3001 levelogger series user guide, 1–85 [online] Available from: https://www.solinst.com/products/dataloggers-and-telemetry/3001-levelogger-series/operating-instructions/user-guide/3001-user-guide.pdf, 2020.

Sundal, A. V., Shepherd, A., Nienow, P., Hanna, E., Palmer, S. and Huybrechts, P.: Melt-induced speed-up of Greenland ice sheet offset by efficient subglacial drainage, Nature, 469(7331), 521–524, doi:10.1038/nature09740, 2011.

Takeuchi, N., Koshima, S., Yoshimura, Y., Seko, K. and Fujita, K.: Characteristics of cryoconite holes on a Himalayan glacier, Yala Glacier Central Nepal, Bull. Glaciol. Res., 17, 51–59, 2000.

Taylor, J.: Introduction to error analysis, the study of uncertainties in physical measurements, University Science Books, Sausalito, California., 1997.

van As, D. and Fausto, R. S.: Programme for Monitoring of the Greenland Ice Sheet (PROMICE): First temperature and ablation records, Geol. Surv. Denmark Greenl. Bull., (23), 73–76, doi:10.34194/geusb.v23.4876, 2011.

van As, D.: Warming, glacier melt and surface energy budget from weather station observations in the melville bay region of northwest greenland, J. Glaciol., 57(202), 208–220, doi:10.3189/002214311796405898, 2011.

van As, D., Hubbard, A. L., Hasholt, B., Mikkelsen, A. B., Van Den Broeke, M. R. and Fausto, R. S.: Large surface meltwater discharge from the Kangerlussuaq sector of the Greenland ice sheet during the record-warm year 2010 explained by detailed energy balance observations, Cryosphere, 6(1), 199–209, doi:10.5194/tc-6-199-2012, 2012.

van As, D., Hasholt, B., Ahlstrøm, A. P., Box, J. E., Cappelen, J., Colgan, W., Fausto, R. S., Mernild, S. H., Mikkelsen, A. B., Noël, B. P. Y., Petersen, D. and van den Broeke, M. R.: Reconstructing Greenland Ice Sheet meltwater discharge through the Watson River (1949–2017), Arctic, Antarct. Alp. Res., 50(1), doi:10.1080/15230430.2018.1433799, 2018.

van de Wal, R. S. W., Boot, W., van den Broeke, M. R., Smeets, C. J. P. P., Reijmer, C. H., Donker, J. J. A. and Oerlemans, J.: Large and Rapid Melt-Induced Velocity Changes in the Ablation Zone of the Greenland Ice Sheet, Science, 321(5885), 111–113, doi:10.1126/science.1158540, 2008.

van den Broeke, M. R., Smeets, C. J. P. P. and Wal, R. S. W. Van De: The seasonal cycle and interannual variability of surface energy balance and melt in the ablation zone of the west Greenland ice sheet, Cryosphere, 5, 377–390, doi:10.5194/tc-5-377-2011, 2011.

van den Broeke, M., Enderlin, E., Howat, I., Kuipers Munneke, P., Noël, B., van de Berg, W. J., van Meijgaard, E. and Wouters, B.: On the recent contribution of the Greenland ice sheet to sea level change, Cryosphere, 10, 1933–1946, doi:10.5194/tc-10-1933-2016, 2016.

van den Broeke, M., Smeets, P., Ettema, J. and Munneke, P. K.: Surface radiation balance in the ablation zone of the west Greenland ice sheet, J. Geophys. Res., 113(D13105), 1-14 doi:10.1029/2007JD009283, 2008.

Van Tricht, K., Lhermitte, S., Lenaerts, J. T. M., Gorodetskaya, I. V., L'Ecuyer, T. S., Noël, B., Van Den Broeke, M. R., Turner, D. D. and Van Lipzig, N. P. M.: Clouds enhance Greenland ice sheet meltwater runoff, Nat. Commun., 7(1), 1–9, doi:10.1038/ncomms10266, 2016.

Wadham, J. L., Hawkings, J., Telling, J., Chandler, D., Alcock, J., O'Donnell, E., Kaur, P., Bagshaw, E., Tranter, M., Tedstone, A. and Nienow, P.: Sources, cycling and export of nitrogen on the Greenland Ice Sheet, Biogeosciences, 13(22), 6339–6352, doi:10.5194/bg-13-6339-2016, 2016.

~~Velicogna, I., Mohajerani, Y., Geruo, A., Landerer, F., Mouginot, J., Noel, B., Rignot, E., Sutterley, T., van den Broeke, M., van Wessem, M. and Wiese, D.: Continuity of ice sheet mass loss in Greenland and Antarctica from the GRACE and GRACE follow-on missions, Geophys. Res. Lett., 47(8), 1–8, doi:10.1029/2020GL087291, 2020.~~

~~Yang, K. and Smith, L. C.: Supraglacial streams on the greenland ice sheet delineated from combined spectral-shape information in high-resolution satellite imagery, IEEE Geosci. Remote Sens. Lett., 10(4), 801–805, doi:10.1109/LGRS.2012.2224316, 2013.~~

Yang, K. and Smith, L. C.: Supraglacial streams on the greenland ice sheet delineated from combined spectral-shape information in high-resolution satellite imagery, IEEE Geosci. Remote Sens. Lett., 10(4), 801–805, doi:10.1109/LGRS.2012.2224316, 2013.

Yang, K. and Smith, L. C.: Internally drained catchments dominate supraglacial hydrology of the southwest Greenland Ice Sheet, J. Geophys. Res. Earth Surf., 121, 1891–1910, doi:10.1002/ 2016JF003927, 2016.

Yang, K., Smith, L. C., Karlstrom, L., Cooper, M. G., Tedesco, M., Van As, D., Cheng, X., Chen, Z. and Li, M.: A new surface meltwater routing model for use on the Greenland Ice Sheet surface, Cryosphere, 12(12), 3791–3811, doi:10.5194/tc-12-3791-2018, 2018.